Density Functional Theory of a New Derivative of Allantoin with Antiplasmodial Properties, Antimycobacterial Activities of Essential Oil from Cordia Batesii WERNHAM (Boraginaceae)

Eric Tiam
Université de Yaoundé I
Dominique Ngono Bikobo
Université de Yaoundé I
Ibrahim Ndassa
Université de Yaoundé I
Norbert Nyemeck II
Université de Yaoundé I
Auguste A Zintchem (augabouem@yahoo.fr)
Université de Yaoundé I
Lawrence Ayong
Centre Pasteur du Cameroun
Patrick Betote Diboué
Institute of Medical Research and Medicinal Plants Studies
Bruno Ndjakou
Université de Yaoundé I
Joséphine Mbing
Université de Yaoundé I
Dieudonné Pegnyemb
Université de Yaoundé I

Research Article

Keywords: Cordia batesii, allantoin, batesiin, NMR and UV spectroscopy, fatty acids, DFT, molecular orbitals, Plasmodium falciparum, Mycobacterium tuberculosis

Posted Date: December 30th, 2020

DOI: https://doi.org/10.21203/rs.3.rs-135025/v1

Version of Record: A version of this preprint was published on March 5th, 2021. See the published version at https://doi.org/10.1186/s13065-021-00742-5.

Density functional theory of a new derivative of allantoin with antiplasmodial properties, antimycobacterial activities of essential oil from *Cordia batesii* WERNHAM (Boraginaceae)

Eric Robert Tiam[1], **Dominique Serge Ngono Bikobo**[1], **Ibrahim Mbouombouo Ndassa**[2,3], **Norbert Mbabi Nyemeck II**[1], **Auguste Abouem A Zintchem**[1,3*], **Lawrence Ayong**[4], **Patrick Hervé Betote Diboué**[5], **Bruno Lenta Ndjakou**[1,3], **Joséphine Ngo Mbing**[1†], **Dieudonné Emmanuel Pegnyemb**[1†].

[1]Department of Organic Chemistry, Faculty of Science, University of Yaoundé I, P.O Box 812, Yaounde, Cameroon;

[2]Department of Inorganic Chemistry, Faculty of Science, University of Yaoundé I, P.O Box 812, Yaounde, Cameroon;

[3]Department of Chemistry, Higher Training College, University of Yaoundé I, P.O Box 47, Yaounde, Cameroon;

[4]Centre Pasteur du Cameroun, Yaounde, Cameroon;

[5]Centre for Research on Medicinal Plants and Traditional Medicine, Institute of Medical Research and Medicinal Plants Studies, Yaounde, Cameroon.

*corresponding author: email: augabouem@yahoo.fr.

[†]these authors contributed equally to this work.

Email addresses:

E. R. Tiam: tim007820030@yahoo.fr
D. S. Ngono Bikobo : ngono_serge@yahoo.fr
I. Mbouombouo Ndassa : indassa@yahoo.fr

N. Mbabi Nyemeck II : mbabi2002@yahoo.fr

Lawrence Ayong: ayong@pasteur-yaounde.org

P. H. Betote Diboué: pbetotedidoue@yahoo.fr

B. Lenta Ndjakou : lentabruno@yahoo.fr

J. Ngo Mbing: jpmbing15@gmail.com

D. E. Pegnyemb : pegnyemb@yahoo.com

Abstract

Background: some chemical and pharmacological investigations were performed on the EtOAc and/or CH_2Cl_2 extracts of the stems of *Cordia batesii* (Boraginaeae); one of its components was subjected to some quantum calculations to get improvement in the understanding of its ^{13}C–NMR and UV properties along with geometric, electronic, thermodynamic data and reactivity descriptors.

Results: a new allantoin (**1**) derivative named batesiin (**2**) was characterized from the EtOAc extract; thirteen known compounds including allantoin (**1**) were either isolated or identified by means of MS, NMR, LC–MS and GC–MS. GC–MS was applied on a fraction of essential oil which was composed of a mixture of fatty acids (**9**–**14**). Density functional theory (DFT) calculations were applied on batesiin (**2**). Data were simulated using B3LYP and MPW1PW91 functionals; calculated chemical shifts at B3LYP/6–31G(d,p) and MPW1PW91/6–31G+(d,p) showed much better correlations with the experimental data. Time dependent DFT applied on **2** at B3LYP/6–31G+(d,p) displayed a major absorption band at λ_{max} = 299.01 nm using chloroform as solvent, 3.01 nm higher than the experimental value. In addition, The MeOH extract of the stems and some isolated compounds were tested *in vitro* against *Pf*7G8 CQS and *Pf* Dd2 CQR strains of *Plasmodium falciparum*; meanwhile, the CH_2Cl_2 extract and the mixture of fatty acids (**9**–**14)** were tested on a resistant mycobacterial strain of *Mycobacterium tuberculosis* codified AC45. Stems disclosed a moderate antiplasmodial activity (IC_{50} = 50 µg/mL) and the mixture **9**–**14** a potent antimycobacterial activity with a MIC = 9.52 µg/mL.

Conclusion: these results tend to emphasize on the use of DFT studies when trying to learn more about the chemical structure through spectroscopic data of a natural compound, especially the case of a derivative of allantoin (**1**); essential oil from *Cordia batesii* presents interesting antimycobacterial activities which need to gain more visibility; further antiplasmodial tests should rely on batesiin (**2**) and other components of the species.

Keywords:

Cordia batesii; allantoin; batesiin; NMR and UV spectroscopy; fatty acids; DFT; molecular orbitals; *Plasmodium falciparum*; *Mycobacterium tuberculosis*.

Introduction

One of the main goals of World Health Organization (WHO) is to end the epidemics of neglected tropical diseases, tuberculosis (TB) and malaria (which remains the major public health and mortality problem in the tropics) by 2030 [1,2]. In 2018, TB infected about 10.0 million people, mainly in WHO regions of South-East Asia (44%), Africa (24%) and the Western Pacific (18%); meanwhile, about 213 million cases of malaria were found in the WHO African region. In the same year, half a million newly rifampicin-resistant TB cases were estimated. In general, 3.4% of new TB cases and 18% of formerly cured patients displayed either multidrugresistant TB or rifampicin-resistant TB (MDR/RR-TB) [3–5]. Chemotherapy has become less effective due to widespread drug-resistant TB, high cost, shortage of drugs for treatment of malaria. Plants are considered to be an important source of major compounds in drug development because of their successful use in treating various human ailments since millenniums. In this context, the search for new natural products from medicinal plants could provide new ways for antimalarial and anti-tubercular drugs. Among these plants, the root decoction of some species of the genus *Cordia* (Boraginaceae) is reported to be useful in the treatment of tuberculosis, bronchitis and malaria [6].

The genus *Cordia* (Boraginaceae) is composed of trees or shrubs and is widespread in Central and South America, India, Asia and Africa [7]. About 350 species of that genus have been identified worldwide, mainly in warmer regions [8]. Previous phytochemical investigations of plants from this genus reported the isolation and characterization of different classes of secondary metabolites including naphthoquinones, hydroquinones [8], cromenes [9], terpenenoids [10] or polyphenols [11]. Meanwhile and based on some pharmacological surveys, essential oils from *C. curassivica* and *C. gilletii* appeared as active against some microbial strains [12,13]

Some biological activities and *in silico* investigations of *C. dichotoma* were recently reported [14,15]; the plant is also known to contain, apart from allantoin (**1**) [16,17] which has been the subject of many quantum calculations [18,19], fatty acids (FA) [20]. FA appear as energy sources for *M. tuberculosis* inside host tissues and are supposed to induce dormancy in *Mycobacterium* bacilli [21,22].

Despite the intensive work performed on some *Cordia* species, no or less investigation has been done on *Cordia batesii* species. In our continuing search for secondary metabolites with potent antiplasmodial and anti-tubercular activities, chemical investigations were carried on the stems of *Cordia batesii*, a forest shrub growing in the central and western regions of Cameroon. This paper describes the isolation of a new derivative of **1** named batesiin (**2**) along with other compounds. A

detailed characterization of **2** was investigated based on NMR and UV–visible spectroscopic analyses and density functional theory (DFT) at B3LYP /6–31G(d,p) [23,24]; 6–31G+(d,p) and MPW1PW91 /6–31G+(d,p) [25,26]. DFT calculations at B3LYP/6–311G++(d,p) were also performed to check some electronic and thermodynamic properties of **2**. Meanwhile, *in vitro* activities regarding extracts of stems and some isolated compounds against two CQR strains of *Plasmodium falciparum* and a resistant mycobacterial strain of *Mycobacterium tuberculosis* were also examined.

Results

Compounds **1**, **3**–**14** were identified based on comparison of their physical and spectral data with authentic samples or those already reported (Fig. 1). Their assignments were consistent with structures of: allantoin (**1**) [15,27], pyrimidine 2,4–(1*H*,3*H*)–dione (**3**) [28], cordialin A (**4**) and cordialin B (**5**) [29], quercetin (**6**) [30], myricetin (**7**) [31], genistein 4'–*O*–glucuronide (**8**) [32], methyl palmitate (**9**) [33], palmitic acid (**10**) [34], methyl (9*E*,12*E*)–octadeca–9,12–dienoate (**11**) [35], methyl oleate (**12**) [36], methyl tridecanoate (**13**) [37] and (*Z*)–octadec–11–enoic acid (**14**) [38].

Characterization of compound 2

Compound **2** was isolated as a white solid from CH_2Cl_2/MeOH mixture. Its molecular formula was deduced as $C_7H_8N_6O_5$ from the ESI–MS signal at *m/z* 257.4 $[M + H]^+$ and from the HR–LC/MS signal at *m/z* 279.1603 $[M + Na]^+$, in accordance with seven degrees of unsaturations. Additional data from the ESI–MS spectrum displayed other peaks at *m/z* 159.4 $[M_1 + H]^+$ and 181.6 $[M_1 + Na]^+$ which are characteristics of allantoin (**1**) [39]. These preliminary data suggested a close relationship between allantoin (**1**) and compound **2**. The ^{1}H–NMR spectrum of **1** exhibited a very prominent peak at δ_H 5.30 (2H, d, ^3J(H,H) = 2.0 Hz, H–C(5)) ppm. Moreover, we observed from the same spectrum some signals attributable to protons attached to heteroatoms (especially to nitrogen) with chemical shifts at δ_H 8.04 [2H, s, H–N(1)], 10.51 [2H, s, H–N(3)], 6.86 [2H, d, ^3J(H,H) = 2.0 Hz, H–N(6)] ppm (Table 1).

The ^{13}C–NMR spectrum of **2** showed four remarkable signals at 157.4 [C(2), 2C], 173.6 [C(4), 2C], 62.4 [C(5), 2C] and 156.8 [C(7), 1C] ppm; when considering that **2** contains seven carbon atoms, the number of aforementioned signals presume the occurrence of a symmetry. The DEPT 135 NMR spectrum of **2** revealed one signal at δ_C 62.4 [C(5)] ppm indicating one methine groups. These observations were confirmed by its HSQC spectrum which indicates a correlation between

the proton at δ_H 5.30 ppm [H–C(5)] and the said carbon. Two remaining signals from the ^{13}C NMR spectrum are observable at δ_C 48.6 and 54.9 ppm and are suggestive of signals of MeOH and CH_2Cl_2 respectively; this assertion is strengthened by correlations between signals at δ_C 48.6 and δ_H 3.17 ppm in one side, and signals at δ_C 54.9 and δ_H 5.74 ppm from the same HSQC spectrum [40].

The HMBC spectrum exhibited noticeable correlations between protons at δ_H 5.30 ppm [H–C(5)] and the carbon atoms at δ_C 173.6 ppm [C(4)] and 156.8 ppm [C(7)], between protons at δ_H 6.88 ppm [H–N(6)] and carbon atoms at δ_C 173.6 [C(4)], 62.4 [C(5)] and 156.8 [C(7)]. Other correlations were found between nitrogenous protons at δ_H 8.04 [H–N(1)] ppm and carbon atoms at δ_C 157.3 ppm [C(2)], δ_C 173.6 ppm [C(4)] and 62.4 ppm [C(5)]. The UV spectrum of **2** (Fig. 2) exhibited one major maximum at λ_{max} = 296 nm, different from values of **1** [19].

Lakshmanan *et al* [39] confirmed through an X–ray analysis that the occurring enantiomer of **1** is its (*S*) one. A thorough analysis of all the spectra and comparison with data from the literature revealed that compound **2** is described for the first time as a new derivative of allantoin (**1**); it was identified as (*S*,*S*)–1,3–bis(2,5–dioxoimidazolidin–4–yl)urea, trivially named batesiin (**2**). Table 1 shows some NMR data of allantoin (**1**) and batesiin (**2**); it strengthens the agreement of a close relationship between those two compounds in terms of NMR spectroscopic data.

DFT calculations of compound 2

The structure of compound **2** was assigned based on spectroscopic analyses including, UV, ^1H– and ^{13}C–NMR, 1D and 2D techniques. To get supplementary detailed awareness into the structure, DFT calculations were completed. The structure of the compound with the right stereochemistry was at first optimized at B3LYP method of DFT using 6–31G(d) basis set. Secondly, conformational analysis [still at B3LYP/6–31G(d)] of the previous optimized structure was applied around the H–C(5)–N(6)–H dihedral angle; this scan led to one optimized geometry for **2**, based on the *cis*–relationship between H–C(5)–N(6)–H (^3J(H,H) = 2.0 Hz). It is shown in Fig. 3 and takes in account previous reports of **1** [39,41]. The five membered ring is almost planar as observed in the case of allantoin (**1**) [19].

The Highest Occupied Molecular Orbital (HOMO) and Lowest Unoccupied Molecular Orbital (LUMO) of compound **2** (Fig. 4) like other descriptors were analyzed at B3LYP/6–311G++(d,p) and compared with those of allantoin (**1**). The calculated HOMO–LUMO gap was 6.532 eV; results are summarized in Table 2.

The ^{1}H– and ^{13}C–NMR spectra of compound **2** were experimentally measured in DMSO–d_6 on 500 and 125 MHz spectrometers respectively. The theoretical NMR were calculated at B3LYP/6–31G(d,p) and MPW1PW91/6–31+G(d,p) in DMSO. The chemical shifts were also simulated at B3LYP/6–31G(d), B3LYP/6–31+G(d,p), MPW1PW91/6–31G(d) and MPW1PW91/6–31G(d,p); however, the correlation with the experiment was relatively weak. GIAO (Gauge Invariant Atomic Orbital) formalism was used during these calculations, and the solvent effect was introduced through polarizable continuum model (PCM) by applying integral equation formalism (IEF). A comparison of the theoretical ^{13}C–NMR values at B3LYP/6–31G(d,p) and MPW1PW91/6–31+G(d,p) with the experimental ones is given in Table 3. A better correlation with the experiment can be achieved if a scaling factor is applied to the ^{13}C–NMR theoretical values.

UV–visible spectrum of **1** displayed two maxima at λ_{max} 183 and 195 nm (representing the absorption bands of amide and imide functions) [19] in one case or a maximum at 265 nm in another case [39]. Despite on the fact that batesiin (**2**) is characterized by the same chromophore groups, its UV–visible spectrum (Fig. 2) exhibits one major absorption band at λ_{max} = 296 nm; the same spectrum exhibits minor absorptions as shoulder sections (letters A and B) with λ_{max} around 287 and 304 nm respectively. Simulated UV–visible spectra of **2** were achieved with chloroform and ethanol as solvents (Fig. 5), based on its tautomeric and ionic forms (Fig. 6): all λ_{max} results (experimental and theoretical) are summarized in Table 4. Excitation energy (in nm) determined in $CHCl_3$ at 283.89 is closed to experimental value at 287 nm while simulation in MeOH exhibits an energy (in nm) at 315.59 which is comparable to the experimental λ_{max} at 304 nm.

Biological properties

The antimalarial potencies screening against *P. falciparum* Dd2 and 7G8 (CQR) strains of the MeOH extract of stems of *C. batesii* and compounds **2**, **3**, **5** and **6** were performed according to the Sybr Green I fluorescence-based assays [42]. The results are presented in Fig.7; they indicate the IC_{50} of extract of stems of *C. batesii* and the percentage of growth inhibition against Dd2 and 7G8 *P. falciparum* strains respectively.

Figure 7**a** showed that the MeOH extract of stems discloses an IC_{50} = 50 µg/mL against Dd2 *P. falciparum* strain which can be considered as a moderate activity. It appears from Fig. 7**b** that, apart from artemisinin (95.75% of inhibition) used as reference, the CH_3OH extract has the highest antiplasmodial activity with 88.24% inhibition percentage followed by **2** with approximately 78% of growth inhibition against Dd2 strain. Compounds **3** and **5** showed high

activity > 65% of inhibition, exhibiting a growth inhibition of Dd2 strain *P. falciparum* with percentage of 66.43% and 72.99% respectively.

When tested against 7G8 *P. falciparum* strain, MeOH extract and compounds **2**, **3** and **5** showed the percentages of growth inhibition of 18.82%, 34.26%, 10.04% and 2.84% at 10 µg/mL respectively. The same extract and isolated compounds at 100 µg/mL, showed 25.03%, 63.86%, 98.07% and – 18.44% of percentages of growth inhibition. These results are summarized in Fig. 7**c** and reveal that **2** and **3** disclose the highest inhibition percentage > 60% on 7G8 *P. falciparum* strains.

From the anti–mycobacterial test results (Table 5), it should be noticed that the mixture of FA (A_1) exhibited a good anti–tubercular activity with a Minimal Inhibitory Concentration (MIC) of 9.52 µg/mL. According to Cantrell *et al*. [43], isolated compounds that exhibit a MIC ≤ 64 µg/mL are considered promising. For crude extracts, the MIC should be ≤ 125 µg/mL [44]. The extract showed poor inhibitory activity against *M*ycobacterium *tuberculosis,* exhibiting a MIC and a Minimal Bactericidal Concentration (MBC) of 1250 and 2500 µg/mL respectively.

Discussion

The high value of the HOMO–LUMO band gap is indicative of a relative stability of the molecule towards oxidation reactions. Plots of frontier orbitals demonstrate that HOMOs and LUMOs are globally focused over the entire molecule; meanwhile, in the case of HOMOs, the ureidyl moiety is less concerned whereas the positive charge is detected over it in LUMOs. The theoretical ^{13}C–NMR values are, on the average, higher than the experimental values. Regardless of the difference in the absolute values, the theoretical values match nicely with the experimental data. Based on the simulated UV–visible spectrum, batesiin (**2**) should most likely appear as an intermediate between various iminols and iminolates groups maybe due to additional stability compared to **1** (Fig. 8). Two protons seem to be located somewhere between, in each case, a nitrogen and an anionic oxygen of the same iminolate group, at a site nearer to oxygen (distance < 1.4 Å) than to nitrogen (distance > 2.3 Å) (Fig. 8). Hence, a virtual loss of symmetry becomes noticeable within **2**, inducing a change in molecular orbitals (MOs) with an impact on electronic transitions (Fig. 9). MOs LUMO and LUMO+1 are localized on an imidazole fragment (especially in the region covering a proton and the anionic oxygen which is near to it) when the other one seems totally unoccupied. When moving from MOs HOMO–1 to HOMO–3, a decrease in the occurrence of MOs in the two imidazole fragments is remarkable and the major electronic density can be found

on the anionic oxygen. Table 4 expresses the nature of electronic transitions which are in accordance with the corresponding λ_{max}.

Results from bioassays against 7G8 *P. falciparum* strain reveal that an increase in concentration (10 to 100 µg/mL) exhibits an increase in percentages of inhibition for MeOH extract of stems, **2** and **3** but a decrease (with a negative percentage) for **5**, which should indicate that the latter is inactive at high concentrations. The moderate activity of the MeOH extract can suggest insufficient synergistic or additive effects of possible anti-plasmodial secondary metabolites from *C. batesii*.

In contrast to the mixture of FA, the weak anti-mycobacterial properties of the crude extract suggest the occurrence within *C. batesii* of components with very poor anti-mycobacterial effects. Moreover, a report from literature reflects that mycobacteria have a lipid–rich hydrophobic cell wall and are often susceptible to less polar compounds [45]. According to Peterson & Shanholtzer [46], bacteriostatic activity has been defined as a ratio of MBC to MIC of > 4. Thus, essential oil exhibited bactericidal activity.

Conclusion

Batesiin (**2**) has been characterized for the first time and its structure was confirmed by DFT at B3LYP/6–31G(d,p) and 6–31G+(d,p) and MPW1PW91/6–31G+(d,p) from this study. Additional data corresponding to HOMO, LUMO, enthalpy, entropy or some reactivity descriptors like IP or EA were also simulated, this time at B3LYP/6–311G++(d,p); moreover, no comparison with the experiment in this case could be made. Simulated energies (in nm) match nicely with experimental data after molecular modelling. The MeOH crude extract of the stems showed a moderate activity against Dd2 *P. falciparum* strain with IC_{50} = 50 µg/mL. The anti-plasmodial properties of batesiin (**2**) and some other compounds are deduced from high percentages of growth inhibition against the 7G8 *P. falciparum* strain; in parallel, anti-tubercular activities against *M. tuberculosis* arise from the mixture of FA (**9**–**14**) with a MIC = 9.52 µg/mL. These results can emphasize the use of *C. batesii* in the treatment of fever or bronchitis by riparians (unpublished data); they suggest that the bioactive principles occurring in the extract, batesiin (**2**) or mixture of FA (**9**–**14**) can be considered as useful templates for further development of new anti–malarial and anti–tubercular drugs respectively. Additional survey should however be performed on **3** to check whether it exhibits other anti-plasmodial properties. Thorough analyses on essential oils from the genus *Cordia* should be conducted to check whether they can be considered as candidates in the fight against tuberculosis.

Methods

General

Melting points were uncorrected and were measured on a Mettler Toledo instrument. IR spectra were recorded on an Alpha FT–IR spectrometer from Bruker, while 1D and 2D NMR spectra were obtained on a Bruker DRX 500 (500 MHz for ^{1}H and 125 MHz for ^{13}C spectra) spectrometer (Bruker, Rheinstetten, Germany) with chemical shifts reported as δ (ppm), using TMS as an internal standard. The ESI–MS were obtained on LTQ–FT instrument (Thermo Scientific). LC–MS were measured with Shimadzu LC–MS system using a L−column 2 ODS (I.D. 2.1 × 100 mm, Chemical Evaluation and Research Institute, Japan), at a flow rate of 0.2 mL min^{-1} with a detection wavelength of 300 nm and FMW (HCOOH/MeCN/H_2O = 1:12:87) as eluent, ESI+ 4.5 kV, ESI− 3.5 kV, 250°C. Optical rotations were measured on a Perkin–Elmer 341 polarimeter. Silica gel 60 (230–400 mesh E. Merck, Darmstadt, Germany) and *Sephadex*® LH–20 were employed for CC, the solvent mixing systems for elution were mainly CH_2Cl_2/MeOH for the phytochemical study with increasing polarity and pure MeOH, while precoated aluminum sheets silica gel 60 F254 were used for TLC [47].

Plant material

The plant material was collected on March 2014 at Koumoul in center region of Cameroon. The identity of plant material was confirmed by the taxonomist Victor Nana. A voucher sample (14106 SRF) is deposited at the National Herbarium of Cameroon, Yaounde.

Extraction and isolation

The stems were dried in shade and cut into small pieces and then submitted for further studies. 80% of air dried pieces of stems of *C. batesii* (500 g) were extracted with MeOH (5 x 500 mL, 30 min each) using an Elma® sonic S 100 at r. t. The extract was filtered; the filtrate was evaporated to dryness in a Rotavapor. The residue obtained from the MeOH extract (about 53 g) was dissolved into hexane-water 80:20 (100 mL) during one day; the resulting hexane-water gum (42 g) was dissolved in a mixture of $CHCl_3$–H_2O 80:20 (100 mL) once again in a period of 24 hours; the resulting $CHCl_3$–H_2O extract (36 g) was dissolved in CH_3COOH–H_2O 70:30 (100 mL) during 24 hours. The final extract (26g) was submitted to further CC analyses. After extraction, the crude MeOH extract (26 g) was subjected to column chromatography of LH–20 (2.5 cm, 50 cm, eluent

MeOH). Four main fractions were obtained: A (10.36 g), B (4.6 g), C (3.0 g) and D (7.0 g). Fraction A (10.36 g) was subjected to a silica gel CC (1.8 cm, 3 x 50 cm, eluent CH_2Cl_2–MeOH 100-1:1) and provided three sub-fraction (A_1, A_2, and A_3). Sub–fraction A_2 (5.20 g) was fractionated by silica gel CC (1.8 cm, 3 x 50 cm, eluent CH_2Cl_2–MeOH 50:1–30:1) to produce two compounds, **4** (4.6 mg) and **5** (11 mg). Fraction B (4.6 g) was chromatographed as described above to give five sub–fractions (B_1, B_2, B_3, B_4 and B_5). Sub–fraction B_1 (0.20 g) was purified by silica gel CC (1.8 cm, 3 x 50 cm, eluent CH_2Cl_2–MeOH 30:1–20:1) to yield compound **1** (9 mg). Compound **2** (7.5 mg) was isolated from sub–fraction B_3 (0.31 g) using a silica gel CC (1.8 cm, 3 x 50 cm, eluent CH_2Cl_2–MeOH 40:1–20:1). Sub–fraction B_4 (0.60 g) was fractionated and purified using a silica gel CC (1.8 cm, 3 x 50 cm, eluent CH_2Cl_2–MeOH 40:1–15:1) to provide **3** (4 mg). The essential oil (sub-fraction A_1, 0.60 g) resulting from the crude extract was analyzed by LC–MS, exhibiting compounds **6**, **7** and **8**. A_1 was soluble in pure hexane and crystallized from pure CH_2Cl_2. 487 mg were analyzed by GC–MS which revealed the compounds **9**, **10**, **11**, **12**, **13** and **14**.

Characteristics of compound 2

Batesiin (**2**), white solid: mp 231–233 ºC. TLC (CH_2Cl_2:MeOH, 20:1 v/v) R_f = 0.6; $[\alpha]_D^{20}$ = – 98.3° (0.04 M in acetone). ^{1}H NMR (500 MHz, DMSO–d_6) δ 10.51 (2H, s, NH), 8.04 (2H, s, NH), 6.88 (2H, d, J = 2 Hz, NH), 5.23 (2H, d, J = 2 Hz); ^{13}C NMR (125 MHz, DMSO–d_6) δ 62.4, 156.8, 157.4, 173.6; IR (KBr) cm^{-1} 3425, 3340 (O–H), 3125, 3060 (N–H), 1810, 1740, 1680, 1560 (C=O); UV/Vis: λ_{max} (MeOH) nm: 296. HR–LC/MS (m/z): $[M+Na]^+$ calcd for $C_7H_8N_6O_5Na^+$; 279.1608; found 279.1603; analysis (calcd., found for $C_7H_8N_6O_5Na$): C (30.12, 30.09); H (2.89, 2.85); N (30.10, 30.10); O (28.66, 28.65).

Computational Details

All calculations were performed with Gaussian 09 suite of programs [48] and UV–visible curves were generated by GaussSum [49]. Geometries were optimized at hybrid B3LYP method using 6–31G(d) basis set (solvent = DMSO). The B3LYP mode provides a good balance between cost and precision. A preliminary predict of the geometry of compound **2** is based on the stereochemistry ascribed through 1D and 2D NMR characterizations. Compound **2** has conformational flexibility around the symmetric dihedral angles H–C(5)–N(6)–H. The dihedral angles around the C(5)–N(6) axe has been scanned at 15 degrees step, to find the lowest energy conformers. A minimum at the dihedral angle of 22.9° was retained because of its conformation closed to the structure of

allantoin (**1**). Afterwards, it was submitted to geometry optimization at B3LYP/6–31G(d) level of theory to provide the optimized geometry of **2** (Fig. **3**). The optimized structure was confirmed by frequency analysis at the same level (B3LYP/6–31G(d)) as a true minimum (no imaginary frequency). Six methods were evaluated for the simulation of ^{1}H– and ^{13}C–NMR spectra; B3LYP/6–31G(d), B3LYP/6–31G(d,p), B3LYP/6–31G+(d,p), MPW1PW91/6–31G(d), MPW1PW91/6–31G(d,p) and MPW1PW91/6–31G+(d,p). The electronic properties at isodensity 0.02 such as Ionization Potential (IP), Electron Affinity (EA), HOMO, LUMO and band gaps were calculated at B3LYP/6-311G++(d,p). The band gap was taken as the difference in energies of HOMO and LUMO. Meanwhile, thermodynamic properties like enthalpy, entropy or molar capacity at constant volume along with reactivity descriptors like chemical potential, electronegativity, hardness, softness were also calculated at B3LYP/6-311G++(d,p). TD–DFT studies were evaluated at B3LYP/6–31G+(d,p) in $CHCl_3$ and in MeOH after a geometry optimization at the same level of theory of the iminolate in Fig. 8. Six steps were then applied to get excitation energies.

Bioassays

***In vitro* cultivation of *P. falciparum* strains**

*Pf*Dd2 and *Pf*7G8 strains of *P. falciparum* were used *in vitro* in blood stage culture to test the antimalarial efficacy of methanol extract of stems of *C. batesii* and isolated compounds **2**, **3** and **5**. The culture was maintained at the Laboratory of parasitology, Centre Pasteur du Cameroon. *P. falciparum* culture was maintained according to the method described by Trager and Jensen [50] with light modifications. *P. falciparum* Dd2 and 7G8 cultures were maintained in fresh O^{+ve} human erythrocytes suspended at 4% haematocrit in RPMI 1640 (Sigma Aldrich – France) containing 0.2% sodium bicarbonate, 0.5% Albumax, 45 µg/L hypoxanthine and 50 µg/L gentamicin, and incubated at 37°C under a gas mixture 5% O_2, 5% CO_2, and 90% N_2. Every day, infected erythrocytes were transferred into fresh complete medium to propagate the culture.

Drug dilutions

Artemisinin (Sigma Aldrich - France) and isolated compounds were prepared in DMSO. All stocks were then diluted with culture medium to achieve the required concentrations. The final solution of all plant extracts, isolated compounds and artemisinin contained 0.4% DMSO, which was found to be non-toxic to the parasites. Drugs and test compounds were then placed in 96–well flat bottom tissue culture grade plates.

Assay for anti-plasmodial activity

The stems of *C. batesii* were evaluated for their antimalarial activity against *P. falciparum* strains Dd2 and 7G8. For drug screening, SYBR green I-based fluorescence assay was setup as described by Smilkstein *et al* [42]. Sorbitol synchronized parasites were incubated under normal culture conditions at 2% haematocrit and 1% parasitemia in the absence or presence of increasing concentrations of methanol extracts of *C. batesii*. artemisinin was used as positive control, while 0.4% DMSO was used as the negative control. After 48 hours of incubation, 100 µL of SYBR Green I solution (0.2 µL/mL of 10,000X SYBR Green I (Sigma Aldrich - France)) in lysis buffer [Tris (20 mM; pH 7.5), EDTA (5 mM), saponin (0.008%; w/v) and Triton X–100 (0.08%; v/v)] was added to each well. The microtiter plate was mixed twice gently with multi-channel pipette and incubated in dark at 37°C for 1 hour. Fluorescence was measured with a fluorescence multi-well plate reader (Perkin Elmer) with excitation and emission wavelength bands centred at 485 and 530 nm, respectively. The fluorescence counts were plotted against the drug concentration and the inhibitory percentage of each plant extract and compound was calculated using the following equation.

$$\text{I}\,(\%) = \frac{\text{Abs control} - \text{Abs extracts/isolated compounds}}{\text{Abs control}} \text{x } 100$$

Where $Abs_{control}$ is the absorbance of untreated well and $Abs_{extracts/isolated\ compounds}$ is the absorbance of extracts or compounds well.

Anti–tubercular tests

For the present study, the mycobacterium (*M. tuberculosis*) used was a clinical isolated strain resistant to isoniazid codified as AC 45 (this strain was obtained from Sangmelima district's Hospital in South Region of Cameroon). The genetical profile of the resistance has been carried out at Laboratory for Tuberculosis Research (Biotechnology Centre, University of Yaoundé I) through Line probe Assay method. The mycobacteria strain has been cultured at 37°C for two weeks in Middlebrook 7H9 (Himedia, India) supplemented with 0.05% (v/v), 2% glycerol and 10% OADC (oleic acid-albumin-dextrose-catalase of Liofilchem s.r.l, Italia). The optical density of 0.45 to 0.55 was measured using spectrophotometer at 550 nm to obtain a suspension of 1.5 x108 UFC/mL. The activity of all phytochemicals (extract and pure compounds) against the aforementioned *M. tuberculosis* strains was tested using the microplate Alamar Blue assay as

described previously by Collins & Franzblau [51]. In a 96 well microplates, all wells received 100 µL of supplemented Middlebrook 7H9 broth, then working metabolites solutions (100 µL) were poured into the first well of each row, from which two–fold dilution series were made through the microplate column. The test inoculum (100 µL) was added to all testing wells, as well as to the drug–free control wells. The final concentration of DMSO in wells was 7% v/v. The final concentrations tested ranged from 250 to 0.244 µg/mL for pure compounds and 5000 to 4.882 µg/mL for extracts. Rifampicin was used as standard drug. Each concentration was assayed in triplicate. Each microplate was sealed with parafilm paper and incubated for 14 days at 37°C. After that, 40 µL of Alamar blue solution was added to two columns of each triplicate in order to show mycobacterial growth and the plates were re–incubated at 37°C for 24 h. After one day of incubation, the MIC was defined as the lowest concentration of phytochemicals that inhibited the bacterial growth (prevents a color change from blue to pink) after incubation time [52]. For the MBC determination, 50 µL of each well which concentration were ≥ MIC was sub–cultured in 150 µL of Mbk 7H9 medium and incubated at 37°C for 10 days, then mycobacterial growth was carried out by addition of 40 µL of alamar blue. MBC was defined as the lowest concentration of extract at which no visible growth of the germ was observed.

Declarations

Ethics approval

Not applicable.

Consent for publication

Not applicable.

Availability of data and materials

All data generated or analyzed during this study are included in this published article (and its supplementary information files).

Competing interests

The authors declare that they have no competing interests.

Funding

The authors acknowledge financial support from the Ministry of Higher Education, Cameroon and from the University of Yaounde I grant committee.

Author's Contribution

E.R. Tiam, N.M. Nyemeck II and P.H. Betote Diboué performed the experiments, D.S.N. Bikobo, I.M. Ndassa and A.A. A Zintchem analyzed the data, conceived and designed the experiments and wrote the article. L. Ayong, B.L. Ndjakou, J.N. Mbing and D.E. Pegnyemb, contributed samples/reagents/materials/analysis tools and analyzed the data. All authors read and approved the final manuscript.

Acknowledgments

We thank Mr Victor Nana for the collection and identification of the plant material. We are indebted to Mr Felix Fehr (Department of Chemistry, University of Fribourg) and to Koert's group (Philipps–Universitat Marburg) for spectral analyses; we also thank the German cooperation through the DAAD/YaBiNaPa program for running the LC–MS analyses.

Supporting information

NMR spectra of compound **2**, some HMBC correlations, GC–MS analyses of compounds **9**, **10**, **11**, **12**, **13** and **14**, LC–MS and GC-MS chromatograms of the extract of *C. batesii*, the ESI–MS spectrum of compound **2**, the genotype profile of *M. tuberculosis* codified AC 45, the shielding tensors of the nuclei of **2**, the electronic (HOMO, LUMO) properties, the Cartesian coordinates of the optimized geometry of compound **2** and TD–DFT are available as supplementary material.

References

1. World Health Organization. Accelerating progress on HIV, tuberculosis, malaria, hepatitis and neglected tropical diseases: a new agenda for 2016-2030. World Health Organization. https://apps.who.int/iris/handle/10665/204419 (2015). Accessed 15 Sep 2020.

2. Rasmussen C., Nyunt MM, Ringwald P. Artemisinin-resistant *Plasmodium falciparum* in Africa. N Engl J Med. 2017;377:305–6.

3. Houben RM & Dodd PJ. The global burden of latent tuberculosis infection: a re-estimation using mathematical modelling. PLoS Med. 2016;13:e1002152.

4. Der Meeren OV, Hatherill M, Nduba V, Wilkinson RJ, Muyoyeta M, Van Brakel E, et al. Phase 2b controlled trial of M72/AS01E vaccine to prevent tuberculosis. N Engl J Med. 2018;379:1621–34.

5. World malaria report. Geneva: World Health Organization; 2019. Licence: CC BY-NC-SA 3.0 IGO.

6. Oza MJ & Kulkarni YA. Traditional uses, phytochemistry and pharmacology of the medicinal species of the genus *Cordia* (Boraginaceae). J P P. 2017;69:755–89.

7. Barroso ICE, de Oliveira F, Ciarelli DM. Morphology of the dispersion unit and germination of *Cordia sellowiana* and *Cordia myxa*. Bragantia. 2009;68:241–9.

8. Ioset JR., Marston A, Gupta MP, Hostettmann K. Antifungal and larvicidal compounds from the root bark of *Cordia alliodora*. J Nat Prod. 2000 ;63 :424–6.

9. Ganjare AB, Nirmal SA, Patil AN. Use of apigenin from *Cordia dichotoma* in the treatment of colitis. Fitoterapia. 2011;82:1052–6.

10. Matos TS, Silva AKO, Quintela AL, Pinto LFC, Canuto KM, Braz-Filho R, et al. Neuroinhibitory meroterpenoid compounds from *Cordia oncocalyx*. Fitoterapia. 2017;123:65–72.

11. Marston A, Zagorski MG, Hostettmann K. Antifungal polyphenols from *Cordia goetzei*. Helv Chim Acta. 1988;71:1210–7.

12. Hernandez T, Canales M, Teran B, Avila O, Duran A, Garcia AM, et al. Antimicrobial activity of the essential oil and extracts of *Cordia curassavica* (Boraginaceae). J Ethnopharmacol. 2007;111:137–41.

13. Okusa PN, Penge O, Devleeschouwer M, Duez P. Direct and indirect antimicrobial effects and antioxidant activity of *Cordia gilletii* De Wild (Boraginaceae). J Ethnopharmacol. 2007;112:476–81.

14. Jamkhande PG, Ghante MH, Barde SR, Ajgunde BR. Antimycobacterial, antimicrobial, antioxidant activities and *in silico* PASS investigations of root fractions and extract of *Cordia dichotoma*. Orient Pharm Exp Med. 2019;19:485–96.

15. Jamkhande PG, Barde SR, Patweker SL, Tidke PS. Plant profile, phytochemistry and pharmacology of *Cordia dichotoma*. Asian Pac J Trop Biomed. 2013;3:1009–12.

16. Tracey MV. Urea and ureides. In: Paech K & Tracey MV, editors. Modern methods of plant analysis. Springer Verlag; 1955. p. 119–141.

17. da Silva VC, de Carvalho MG, Alves AN. Chemical constituents from leaves of *Palicourea coriacea* (Rubiaceae). J Nat Med. 2008;62:356–7.

18. Kus N, Bayar SH, Fausto R. Thermal decomposition of allantoin as probed by matrix isolation FTIR spectroscopy. Tetrahedron 2009;65:9719–27.

19. Alam MJ & Ahmad S. FTIR, FT–Raman, UV–visible spectra and quantum chemical calculations of allantoin molecule and its hydrogen bonded dimers. Spectrochim Acta A 2015;136, 961–78.

20. Nariya PB, Shukla VJ, Acharya RN, Nariya MB, Dhalani JM, Patel AS, Ambasana PA. Triterpenoid and fatty acid contents from the stem bark of *Cordia dichotoma*. Folia Med (Plovdiv). 2018;60:594-600.

21. McKinney JD, Höner zu Bentrup K, Muñoz-Elías EJ, Miczak A, Chen B, Chan WT, Swenson D, Sacchettini JC, et al. Persistence of *Mycobacterium tuberculosis* in macrophages and mice requires the glyoxylate shunt enzyme isocitrate lyase. Nature. 2000;406:735–8.

22. Arai M, Yamano Y, Kamiya K, Setiawan A, Kobayashi M. Anti-dormant mycobacterial activity and target molecule of melophlins, tetramic acid derivatives isolated from a marine sponge of *Melophlus* sp. J Nat Med. 2016;70:467–75.

23. Becke DA. Density–functional thermochemistry. III. The role of exact exchange. J Chem Phys. 1993;98:5648–52.

24. Lee C, Yang W, Parr RG. Development of the Colle–Salvetti correlation–energy formula into a functional of the electron density. Phys Rev B. 1988;37:785–9.

25. Adamo C & Barone V. Exchange functionals with improved long-range behavior and adiabatic connection methods without adjustable parameters: The *m*PW and *m*PW1PW models. J Chem Phys. 1998;108:664–75.

26. Perdew JP, Chevary JA, Vosko SH, Jackson KA, Pederson MR, Singh DJ, Fiolhais C. Atoms, molecules, solids, and surfaces: Applications of the generalized gradient approximation for exchange and correlation. Phys Rev B. 1992;46:6671–87.

27. Zeukang RD, Noundou XS, Fotsing MT, Kuiate TT, Mbafor JT, Krause RWM, et al. Cordidepsine is a potential new anti-HIV depsidone from *Cordia millenii*. Molecules. 2019;24:3202–16.

28. Li P, Feng ZX, Ye D, Huan W, Gang WD, Dong LX. Chemical constituents from the whole plant of *Euphorbia altotibetic*. Helv Chim Acta 2003;86:2525–32.

29. Velde VV, Lavie D, Zelnik R, Matida AK, Panizza S. Cordialin A and B, two new triterpenes from *Cordia verbenacea*. J Chem Soc Perkin Trans 1. 1982;2697–2700.

30. Formica JV & Regelson W. Review of the biology of quercetin and related bioflavonoids. Food Chem Toxicol. 1995;33:1061–80.

31. Hergert HL. The flavonoids of lodgepole pine bark. J Org Chem. 1956;21:534–7.

32. Coughlin JL, Winnik B, Buckley B. Measurement of bisphenol A, bisphenol A β–D-glucuronide, genistein, and genistein 4′–β–D–glucuronide via SPE and HPLC–MS/MS. Anal Bioanal Chem. 2011;401:995–1002.

33. Deliy IV, Vlasova EN, Nuzhdin AL, Gerasimov EY, Bukhtiyarova, GA. Hydrodeoxygenation of methyl palmitate oversulfided Mo/Al_2O_3, $CoMo/Al_2O_3$ and $NiMo/Al_2O_3$ catalysts. RSC Adv. 2014;4:2242–50.

34. Gao H, Hong K, Zhang X, Liu HW, Wang NL, Zhuang L, Yao XS. New steryl esters of fatty acids from the mangrove fungus *Aspergillus awamori*. Helv Chim Acta. 2007;90:1165–78.

35. El-Shouny WA, Ali SS, Sun J, Samy SL, Ali A. Drug resistance profile and molecular characterization of extended spectrum beta–lactamase (ESβL)–producing *Pseudomonas aeruginosa* isolated from burn wound infections; essential oils and their potential for utilization. Microb Pathog. 2018;116:301–12.

36. Kazi SA, Clark P, Campi EM, Jackson WR, Hearn MTW. Metathesis reactions with a low–cost spinning disk system. Green Chem Lett Rev. 2019;12:407–19.

37. Azuma CM, dos Santos FCS, Lago JHG. Flavonoids and fatty acids of *Camellia japonica* leaves extract. Braz Pharmacogn. 2011;21:1159–62.

38. Nie Y & Stürzenbaum SR. Model nematodes. In: obesity research in animal models for the study of human disease: second Edition. Elsevier Inc; 2017. p. 267–280.

39. Lakshmanan G, Sivaraj C, Ammar A, Krishnan DA, Gopinath S, Saravanan K, et al. Isolation and structural elucidation of allantoin, a bioactive compound from *Cleome viscosa*: a combined experimental and computational investigation. Pharmacogn J. 2019;11:1391–1400.

40. Fulmer GR, Miller AJM, Sherden NH, Gottlieb HE, Nudelman A, Stoltz BM, et al. NMR chemical shifts of trace impurities: common laboratory solvents, organics, and gases in deuterated solvents relevant to the organometallic chemist. Organometallics. 2010;29:2176–9.

41. Mootz D. The crystal structure of DL–allantoin. Acta Cryst. 1965;19:726–34.

42. Smilkstein M, Sriwilaijaroen N, Kelly JX, Wilairat D, Riscoe M. Simple and inexpensive fluorescence based technique for high–throughput antimalarial screening. Antimicrob Agents Chemother. 2004;48:1803–6.

43. Cantrell CL, Franzblau SG, Fischer NH. Antimycobacterial plant terpenoids. Planta Med. 2001;67:685–694.

44. Gu JQ, Wang Y, Franzblau SG, Montenegro G, Yang D, Timmermann, BN. Antitubercular constituents of *Valeriana laxiflora*. Planta Med. 2004;70:509–14.

45. Pauli GF, Case RJ, Inui T, Wang Y, Cho S, Fischer NH, Franzblau SG. New perspectives on natural products in TB drug research. Life Sci. 2005;78:485–94.

46. Peterson LR & Shanholtzer C.J. Tests for bactericidal effects of antimicrobial agents: technical performance and clinical relevance. Clin Microbiol Rev. 1992;5:420–32.

47. Tiam ER, Dominique Bikobo DS, Abouem A Zintchem A, Mbabi Nyemeck II N, Moni Ndedi EDF, Betote Diboué PH, et al. Secondary metabolites from *Triclisia gilletii* (Menispermaceae) with antimycobacterial activity against *Mycobacterium tuberculosis*. Nat Prod Res. 2019;33:642–50.

48. Frisch MJ, Trucks GW, Schlegel HB, Scuseria GE, Robb MA, Cheeseman JR, et al. Gaussian 09, Revision B.01, Gaussian, Inc., Wallingford CT. 2010.

49. O'Boyle NM, Tenderholt AL, Langner KM. J Comp Chem. 2008;29:839–45.

50. Trager W & Jensen JB. Human malaria parasites in continuous culture. Science. 1976;193:673–5.

51. Collins L & Franzblau SG. Microplate alamar blue assay versus BACTEC 460 system for high–throughput screening of compounds against *Mycobacterium tuberculosis* and *Mycobacterium avium*. Antimicrob Agents Chemother. 1997;41:1004–9.

52. CLSI. *Susceptibility testing of Mycobacteria, Nocardiae, and other aerobic actinomycetes–Second Edition*, Approved Standard M24–A2 Wayne, PA: Clinical and Laboratory Standards Institute. 2011.

53. Coxon B, Fatiadi AJ, Sniegoski LT, Hertz HS, Schaffer R. A novel acylative degradation of uric acid, Carbon–13 nuclear magnetic resonance studies of uric acid and its degradation products. J Org Chem. 1977;42:3132–40.

54. Asia NR, Fatma UA, Mayades S, Mutasem OT. Investigation of the active constituents of *Portulaca oleraceae* (Portulacaceae) growing in Jordan. Pak J Pharm Sci. 2004;17:37–45.

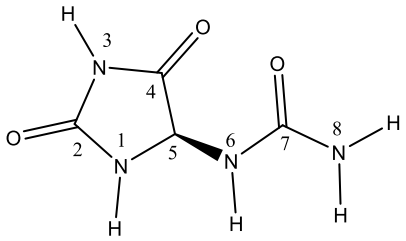

1

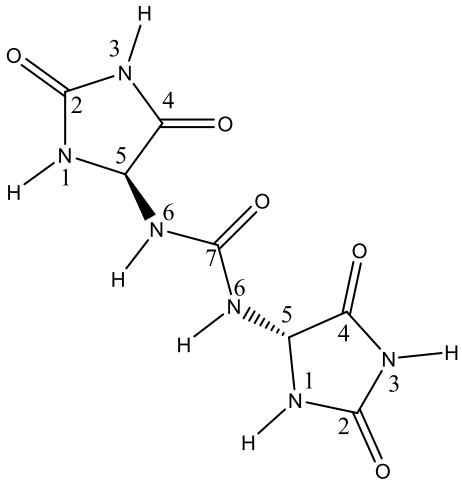

2

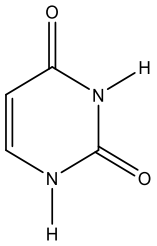

3

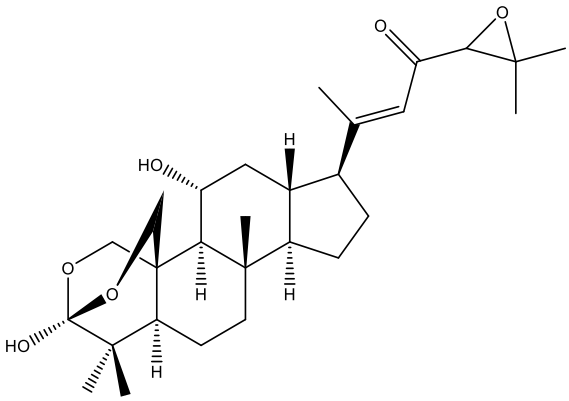

4

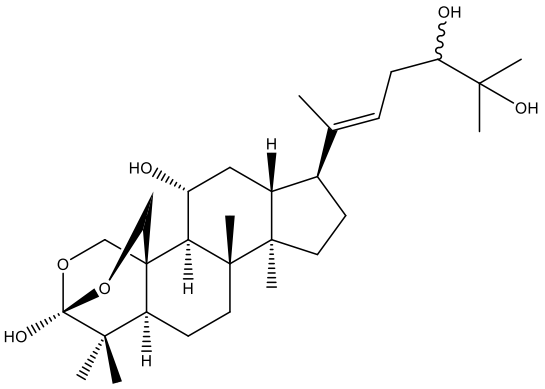

5

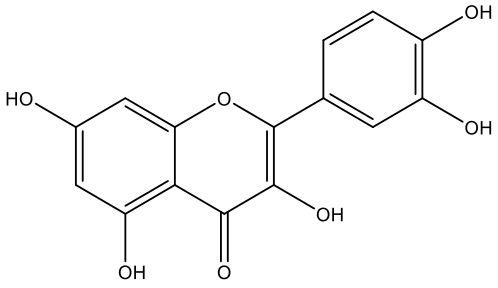

6

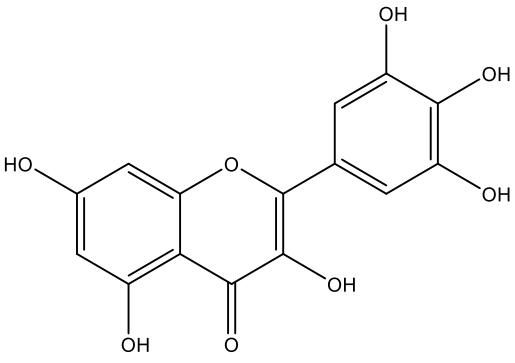

7

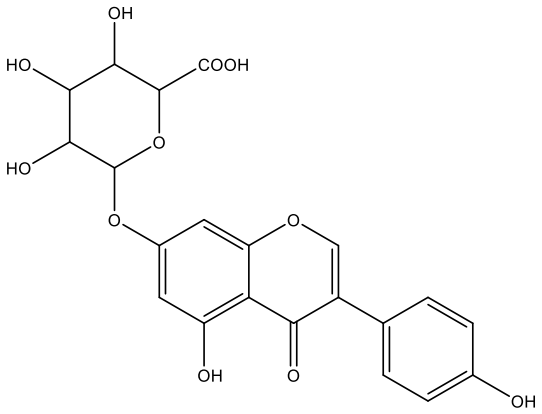

8

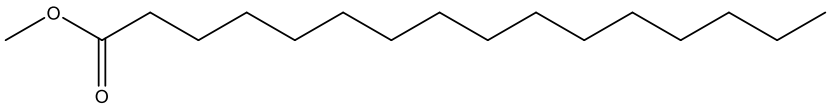

9

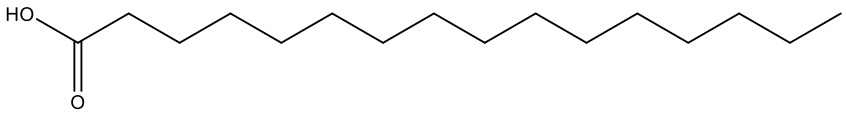

10

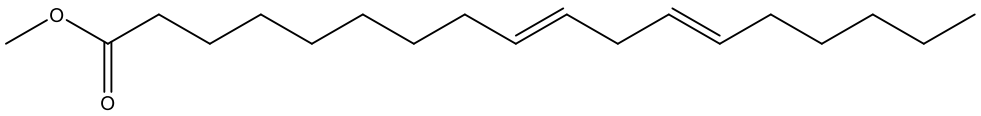

11

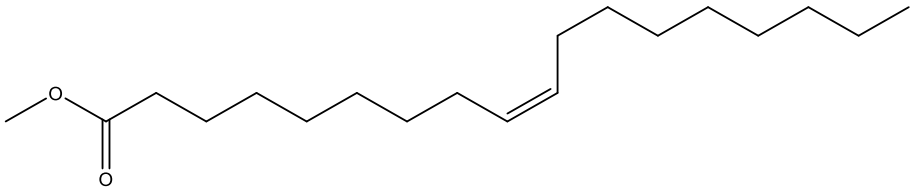

12

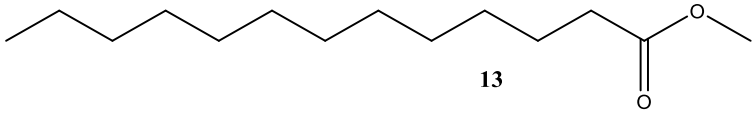

13

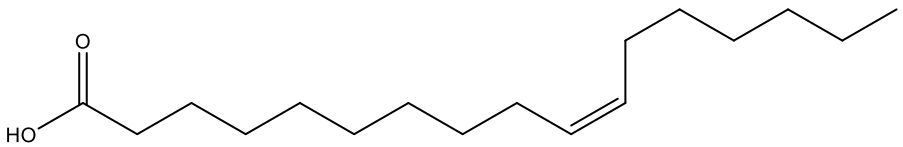

14

Fig. **1**. Structures of the isolated compounds (**1-14)** from the stems of *C. batesii*.

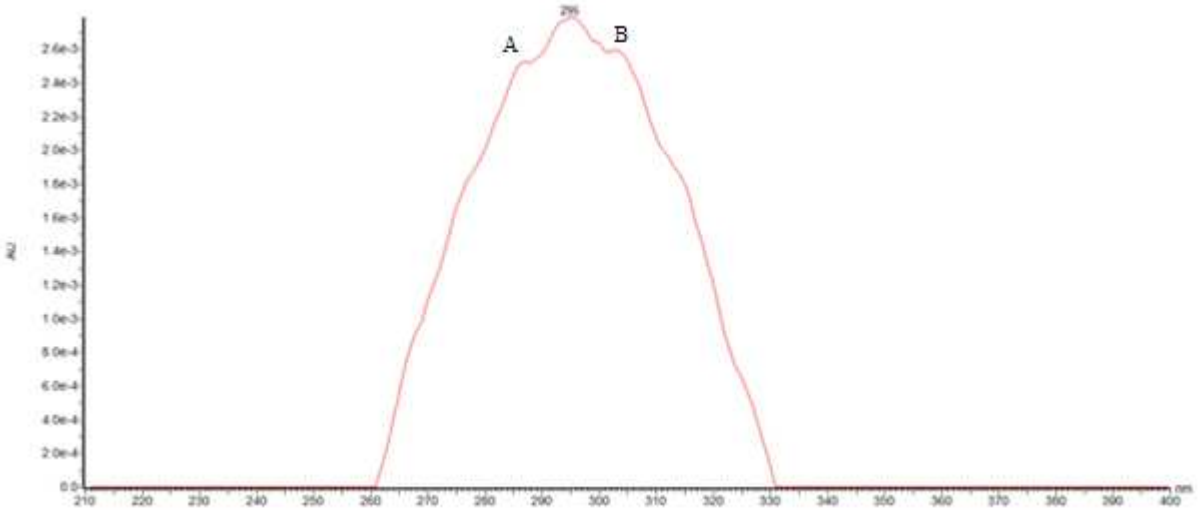

Fig. **2**: UV–visible spectrum of batesiin (**2**).

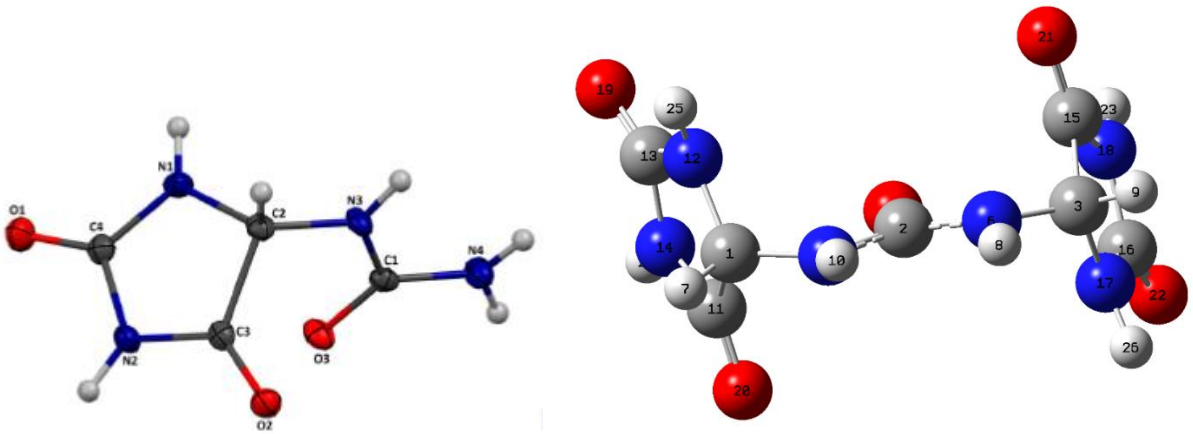

(3**a**) (3**b**)

Fig. 3. (3**a**) ORTEP diagram of allantoin (**1**) [40]; (3**b**) optimized geometry of batesiin (**2**) at B3LYP/6–31G(d).

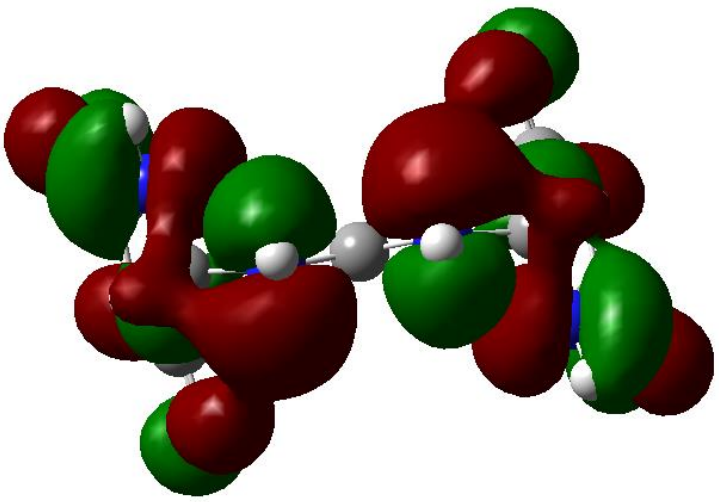

(4**a**)

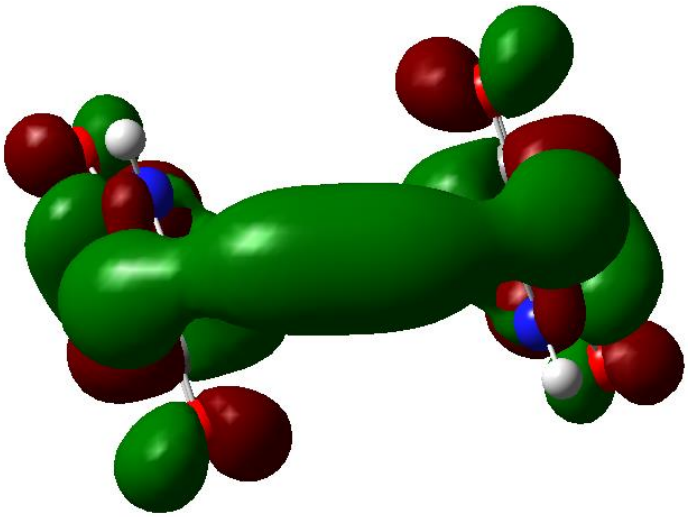

(4**b**)

Fig. 4: (4**a**) HOMO; (4**b**) LUMO of **2**, calculated at B3LYP/6–311G++(d,p). The orbitals are plotted at isodensity of 0.02.

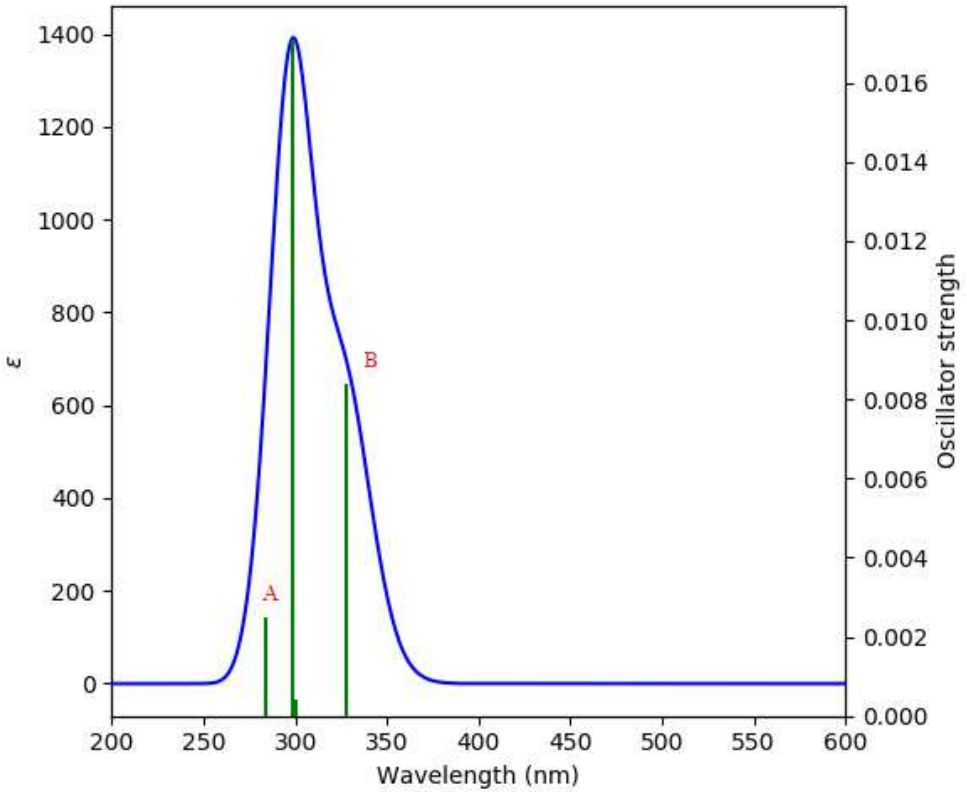

(5**a**)

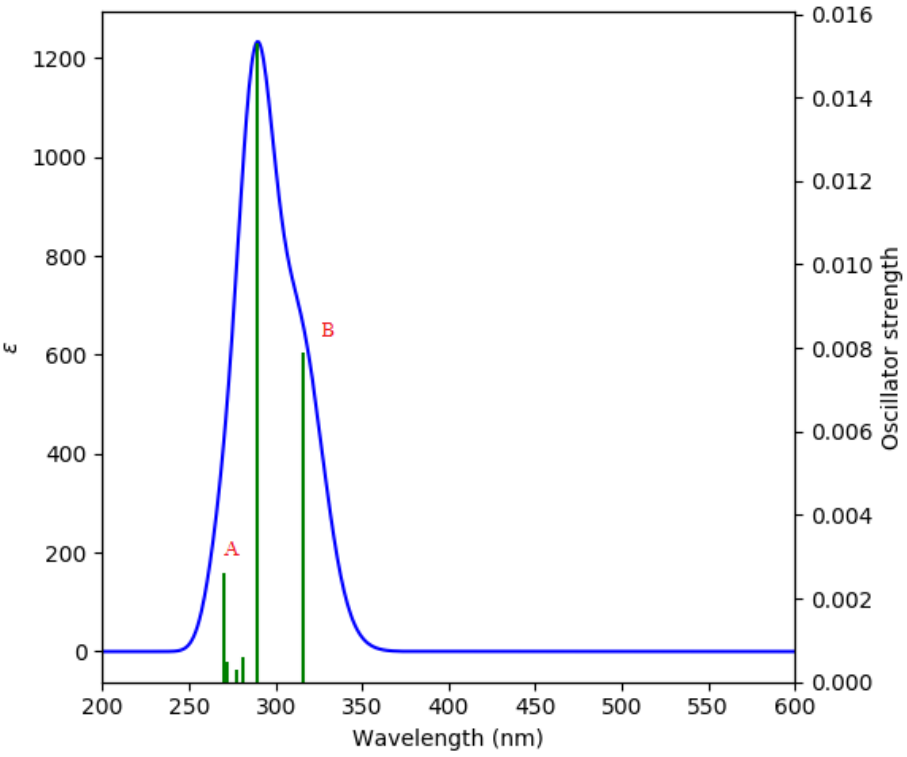

(5**b**)

Fig. 5: simulated UV–visible spectra of **2** (7**a**) in chloroform; (7**b**) in ethanol, at B3LYP/6–31G+(d,p).

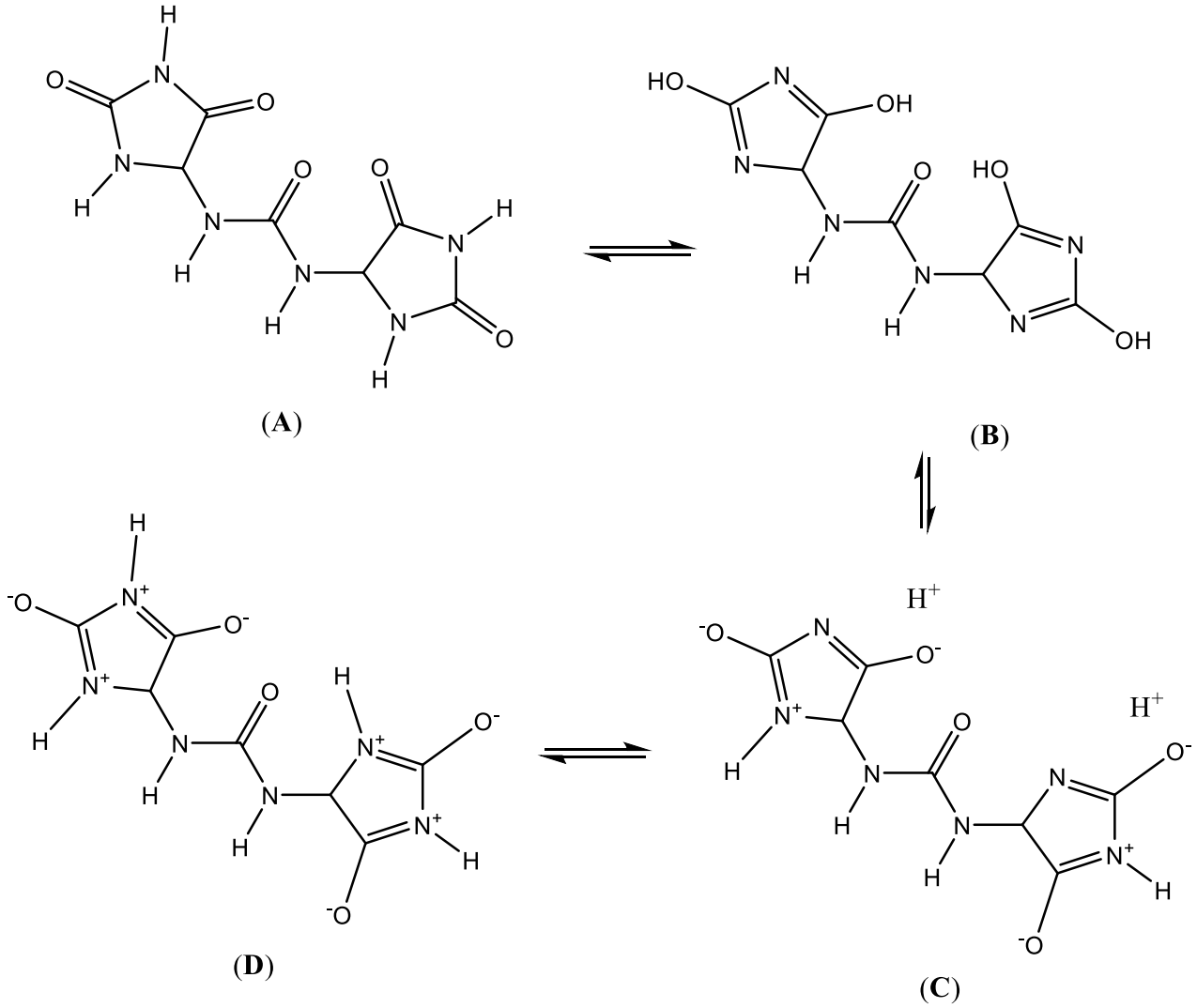

Fig. 6: tautomeric and ionic forms of **2**; based on UV–visible results, it seems most likely that the (**C**) form should be the major one.

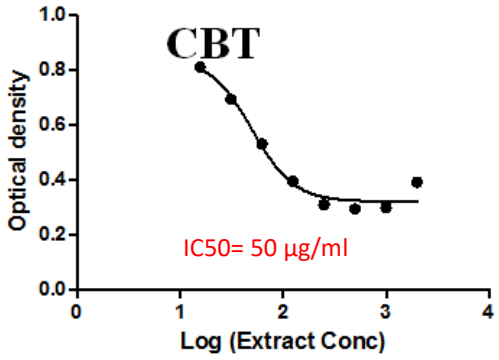

(7**a**)

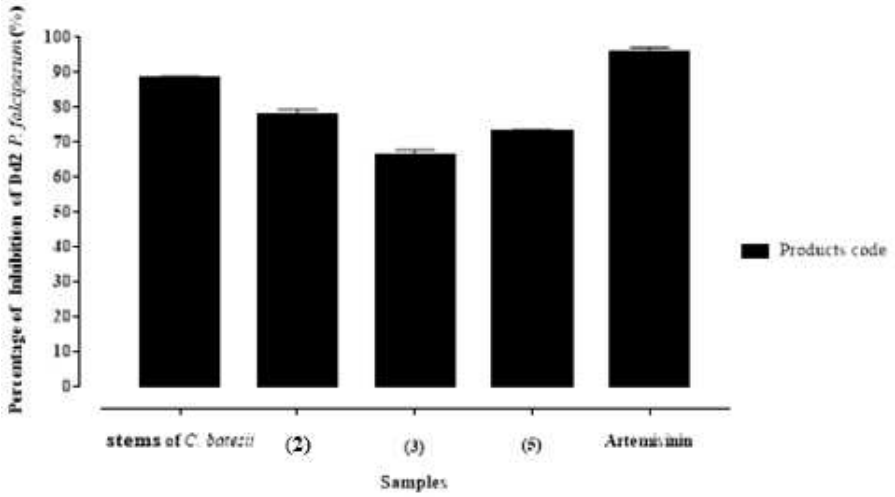

(7**b**)

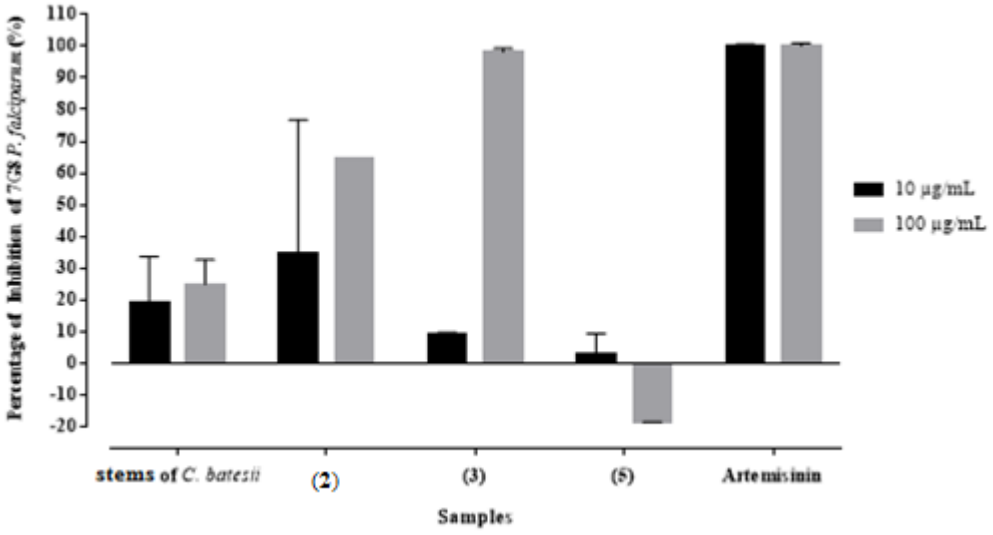

(7**c**)

Fig. 7: (7**a**) result of 2–fold dose response analysis of the extract of *C. batesii* against Dd2 *P. falciparum* strain; (7**b**) Inhibition percentage of stems of *C. batesii* and isolated compounds against *P. falciparum* Dd2 strain; (7**c**) Inhibition percentage of stems of *C. batesii* and isolated compounds against *P. falciparum* 7G8 strain.

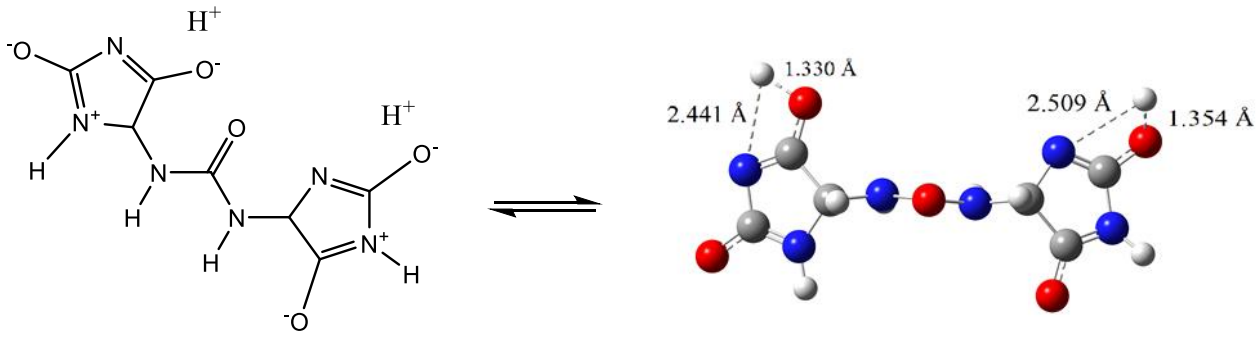

Fig. 8. One case of simulated "iminol"/"iminolate" form of **2** with distances between protons and nitrogen or oxygen atoms at B3LYP/6–31G+(d,p); this form seems to induce the electronic transitions (in nm).

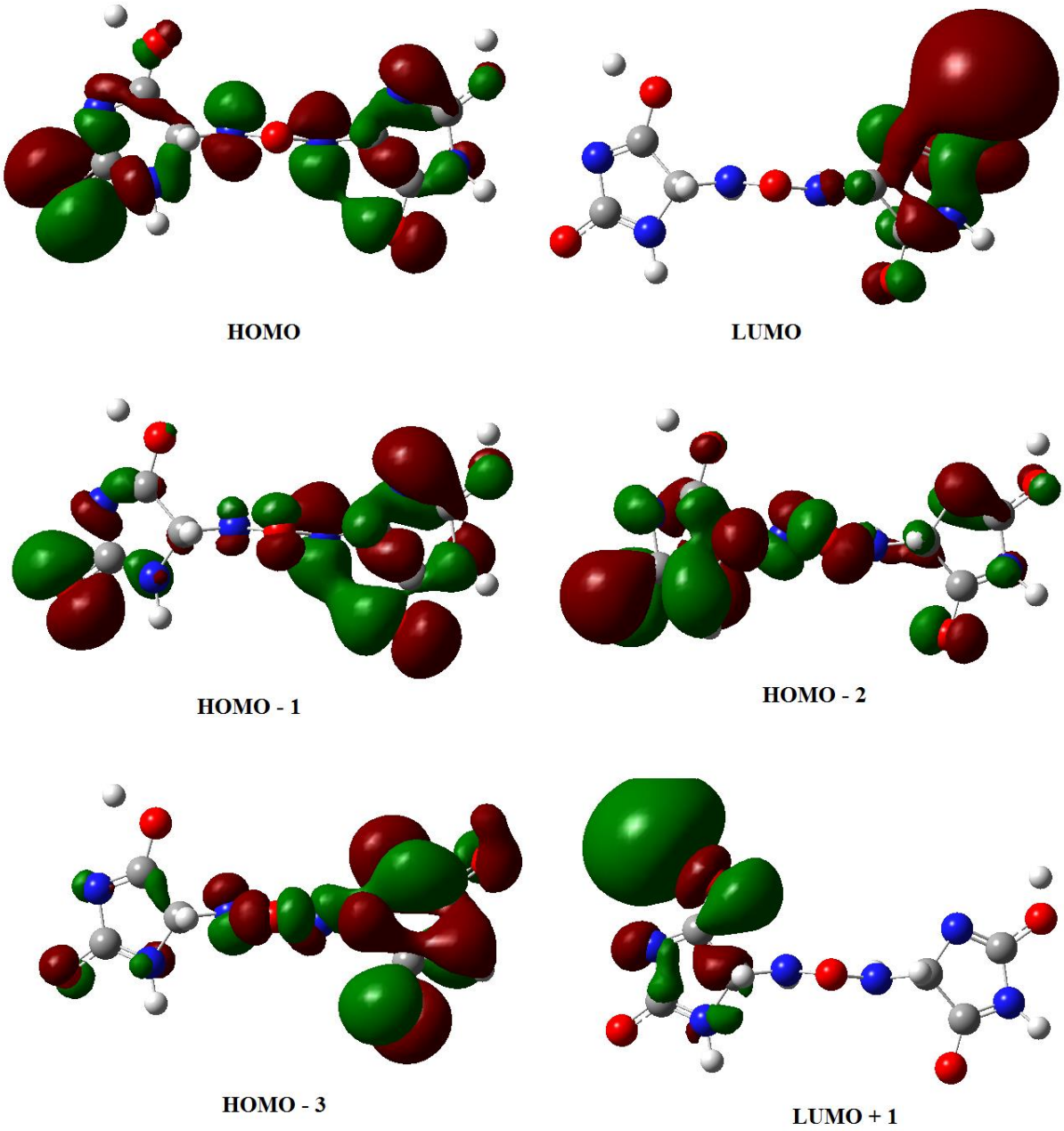

Fig. 9: various MOs of **2** involved in electronic transitions, at B3LYP/6–31G+(d,p).

Table 1: ^{1}H– and ^{13}C–NMR 1D and 2D spectroscopic data of **1** and **2** (500 and 125 MHz in DMSO–d_6) in ppm**.**

Position	allantoin (**1**) [53,54]		batesiin (**2**)	
	δC	**δH**	**δC**	**δH** (m, *J*)
2	156.7	-	156.8	-
4	62.3	5.23	62.4	5.30 (d, 2.0 Hz, 2H)
5	173.4	-	173.6	-
7	157.4	-	157.4	-
H–N(1)	-	8.04	-	8.04 (s, 2H)
H–N(3)	-	10.62	-	10.51 (s, 2H)
H–N(6)	-	6.88	-	6.88 (2H, d, 2.0 Hz)

Table 2. Some electronic and thermodynamic results of batesiin (**2**) compared to data of allantoin (**1**) at B3LYP/6–311G++(d,p). The values are calculated in solution phase (at 298.15 K).

Parameters	allantoin (**1**) [20]	batesiin (**2**)
SCF Energy (a.u.)	– 600.99534493	– 976.613456279
Zero point vibrational energy (kcal mol^{-1})	77.961	116.28268
Rotational constants (GHz)		
	1.876	0.76108
	0.876	0.24433
	0.754	0.23602
Rotational temperatures (Kelvin)		
	0.090	0.03653
	0.042	0.01173
	0.036	0.01133
Total energy (thermal) (*kcal* mol^{-1})	84.462	126.022
Molar heat capacity at constant volume, c_v (*cal* mol^{-1} K^{-1})	37.756	58.650
Molar heat capacity at constant pressure, c_p (*cal* mol^{-1} K^{-1})	39.744	60.639
Total entropy, S (*cal* mol^{-1} K^{-1})	100.182	126.868
Total enthalpy, H (*kcal* mol^{-1})	85.055	126.614
Frontier MO Energies (eV)		
E_{LUMO}	– 1.196	– 1.203
E_{HOMO}	– 7.456	– 7.735
$E_{LUMO} - E_{HOMO}$	6.260	6.532
Global reactivity descriptors		
Ionization potential, *IP* (*eV*)	7.456	7.735
Electron affinity, *EA* (*eV*)	1.196	1.203
Electronegativity, χ	4.326	4.469
Chemical potential, μ	– 4.326	– 4.469
Hardness, η	3.130	3.266
Softness, *S*	0.160	0.153

Table 3. Experimental and calculated [at B3LYP/6–31G(d, p) and MPW1PW91/6–31+G(d,p)] ^{13}C–NMR data of **1**.

Position	**^{13}C chemical shifts (ppm)**		
	Experimental	B3LYP/6–31G(d,p)	MPW1PW91/6–31+G(d,p)
2	156.8	156.1	157.0
4	173.6	174.4	174.6
5	62.4	61.7	62.7
7	157.4	157.0	158.0

Table **4**: main experimental and vertical excitation energies of batesiin (**2**) along with oscillator strengths and transitions

Experimental	Excitation energy (nm)		Oscillator strength		Electronic transition	
	$CHCl_3$	EtOH	$CHCl_3$	EtOH	$CHCl_3$	EtOH
287	283.89	270.11	0.0025	0.0026	^{a}H–2 → ^{b}L+1	^{a}H–2 → ^{b}L+1
296	299.01	289.70	0.0171	0.0153	^{a}H–3 → ^{b}L	^{b}H–3 → ^{b}L
304	327.69	315.59	0.0084	0.0079	^{a}H–1 → ^{b}L	^{a}H–1 → ^{b}L

^{a}H: HOMO

^{b}L: LUMO

Table 5. MIC and MBC values of the methanol extract and the mixture of fatty acids (A_1) against *Mycobacterium tuberculosis* (AC 45).

Plant species	**MIC^{a} (µg/mL)**	**MBC^{b} (µg/mL)**	**MBC/MIC**
C. batesii	1250	2500	2
A_1	9,52	38,25	4
RMP	0.97	7.81	8

^{a}Minimum Inhibitory Concentration

^{b}Minimum Bactericidal Concentration

RMP = Rifampicin

Figures

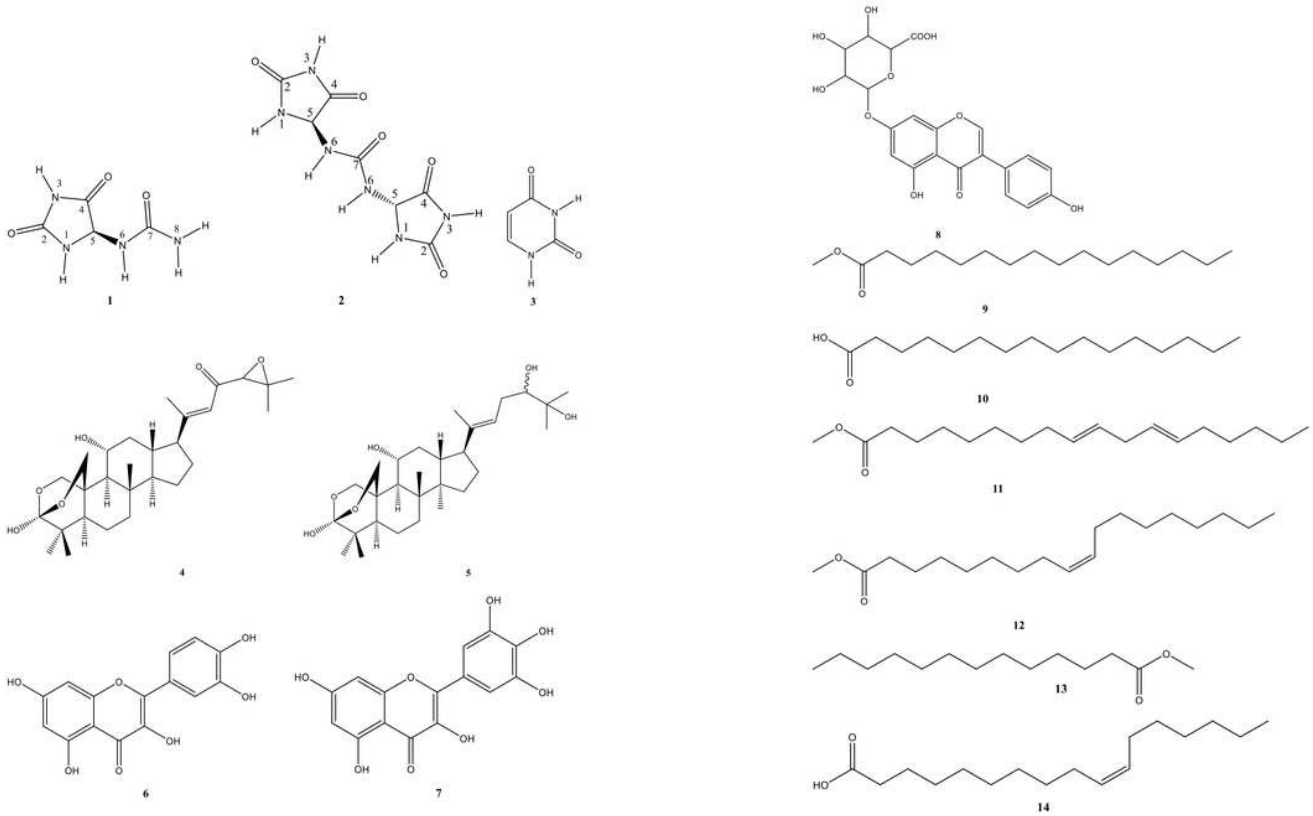

Figure 1

Structures of the isolated compounds (1-14) from the stems of C. batesii.

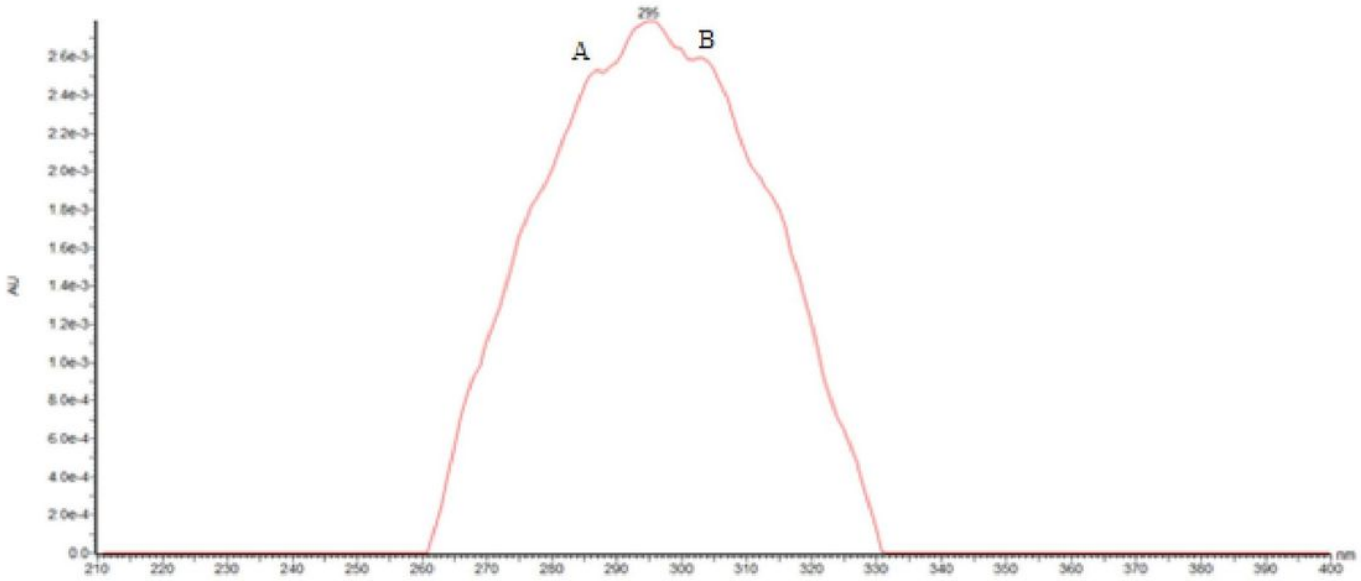

Figure 2

UV–visible spectrum of batesiin (2).

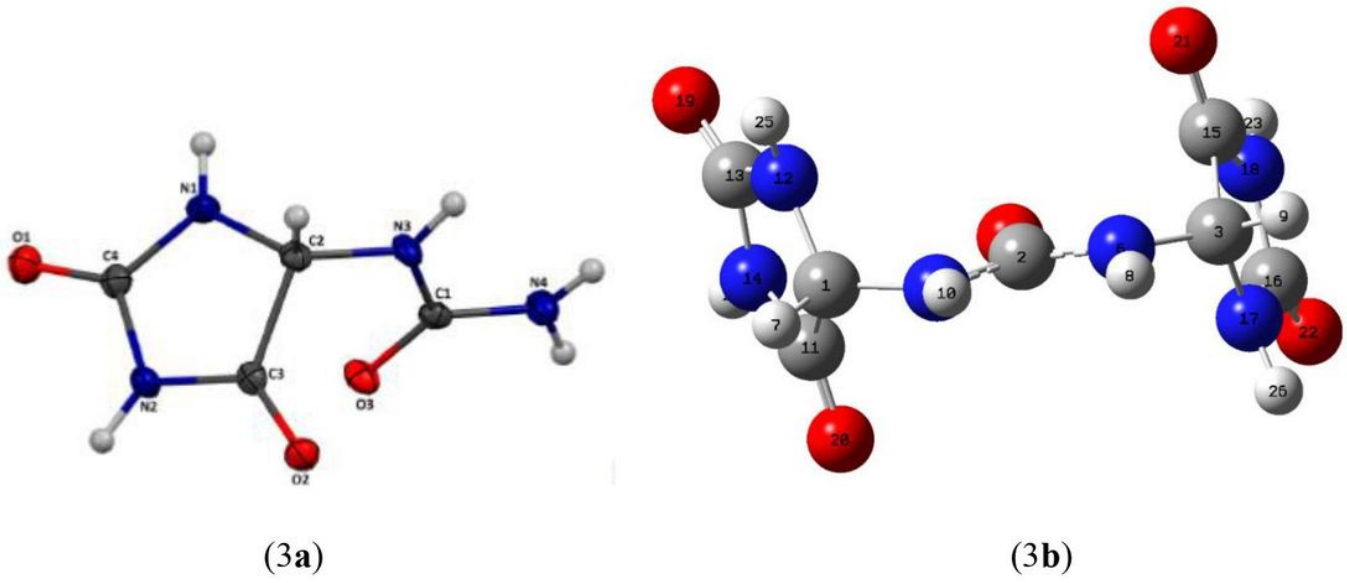

Figure 3

(3a) ORTEP diagram of allantoin (1) [40]; (3b) optimized geometry of batesiin (2) at B3LYP/6–31G(d).

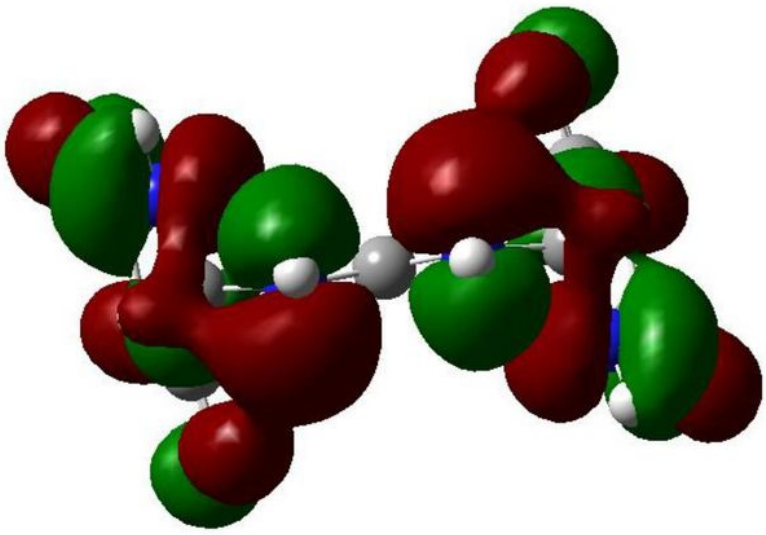

(4a)

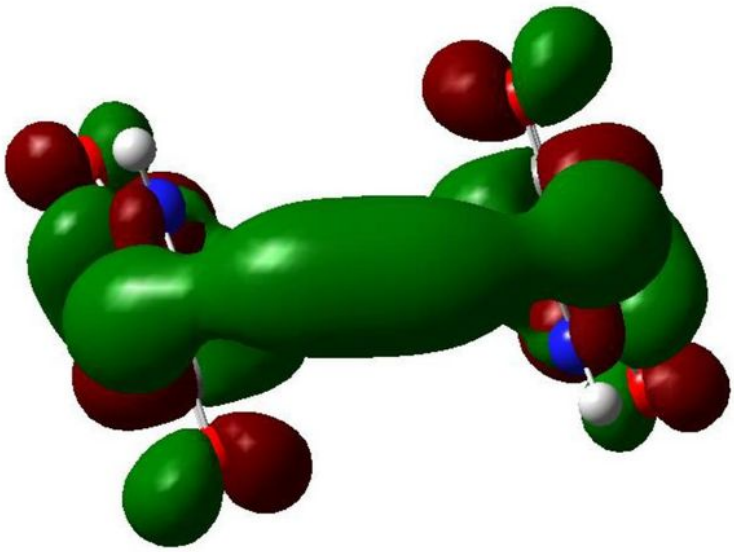

(4b)

Figure 4

(4a) HOMO; (4b) LUMO of 2, calculated at B3LYP/6–311G++(d,p). The orbitals are plotted at isodensity of 0.02.

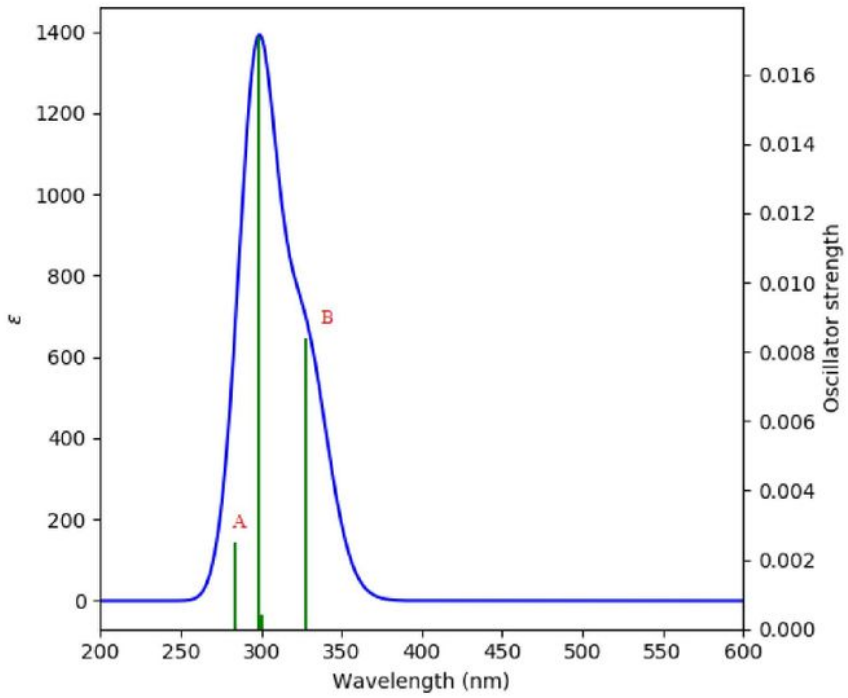

(5a)

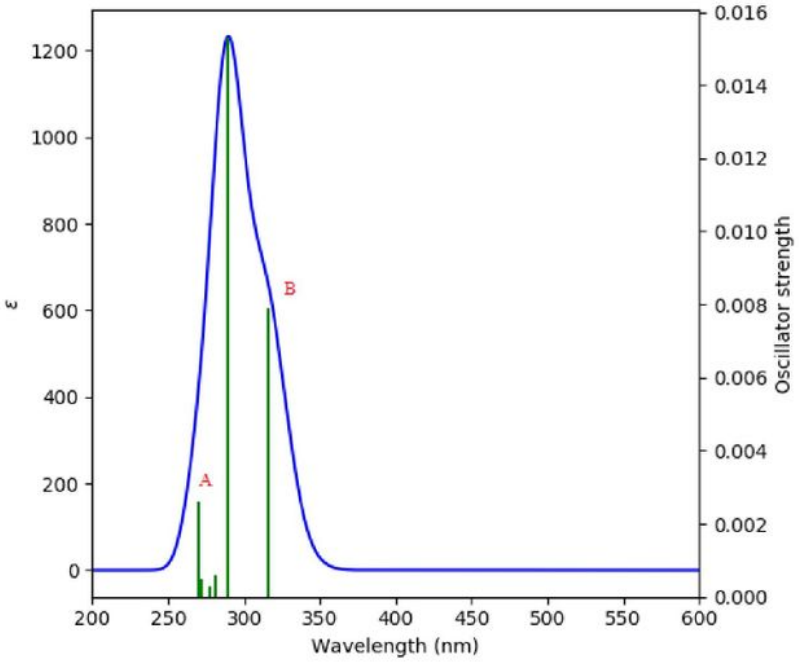

(5b)

Figure 5

simulated UV–visible spectra of 2 (7a) in chloroform; (7b) in ethanol, at B3LYP/6–31G+(d,p).

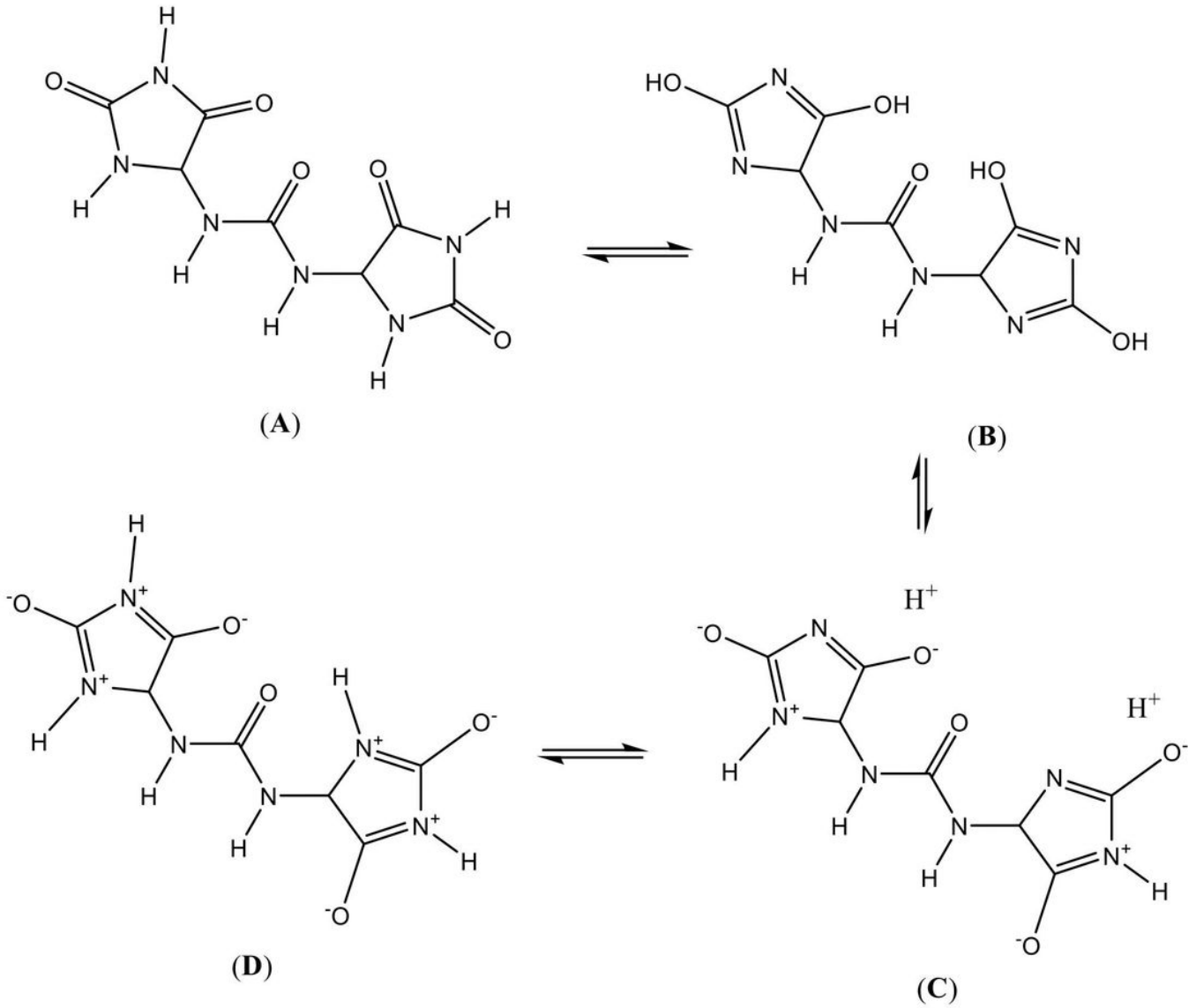

Figure 6

tautomeric and ionic forms of 2; based on UV–visible results, it seems most likely that the (C) form should be the major one.

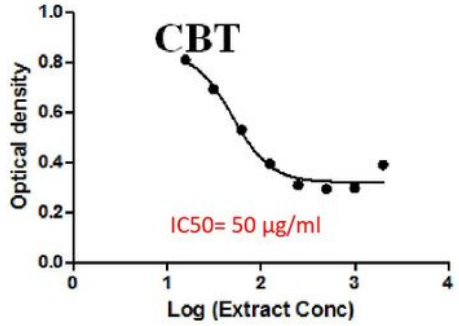

(7a)

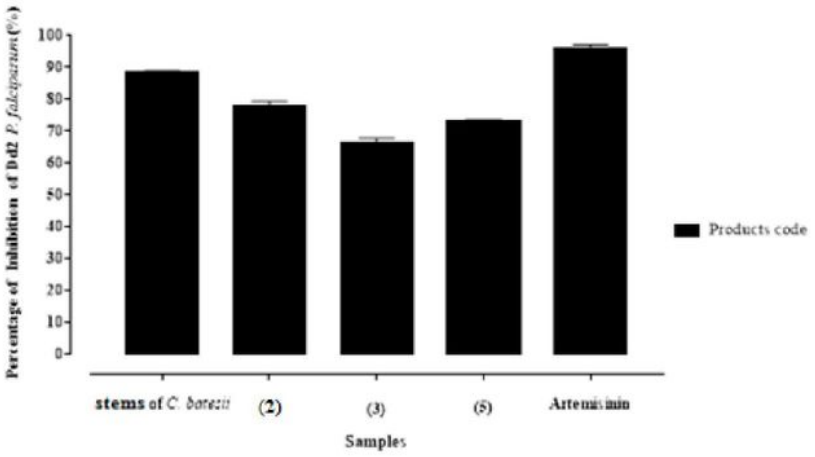

(7b)

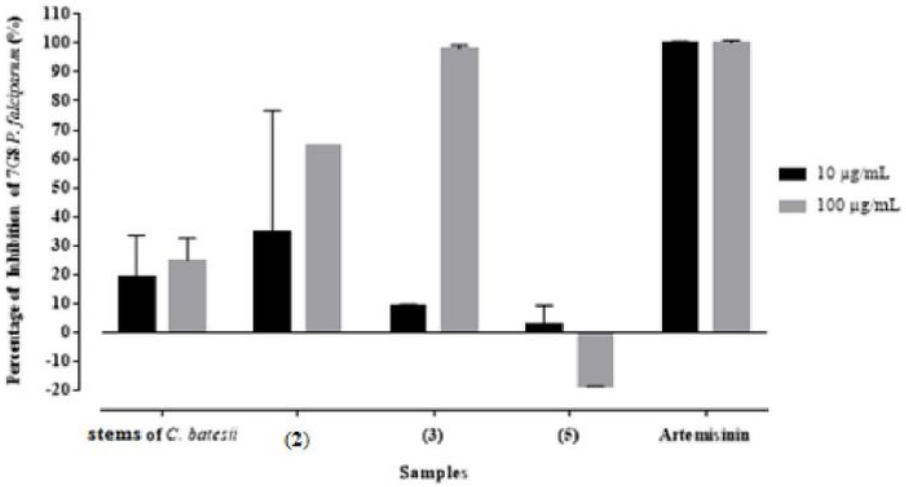

(7c)

Figure 7

(7a) result of 2–fold dose response analysis of the extract of C. batesii against Dd2 P. falciparum strain; (7b) Inhibition percentage of stems of C. batesii and isolated compounds against P. falciparum Dd2 strain; (7c) Inhibition percentage of stems of C. batesii and isolated compounds against P. falciparum 7G8 strain.

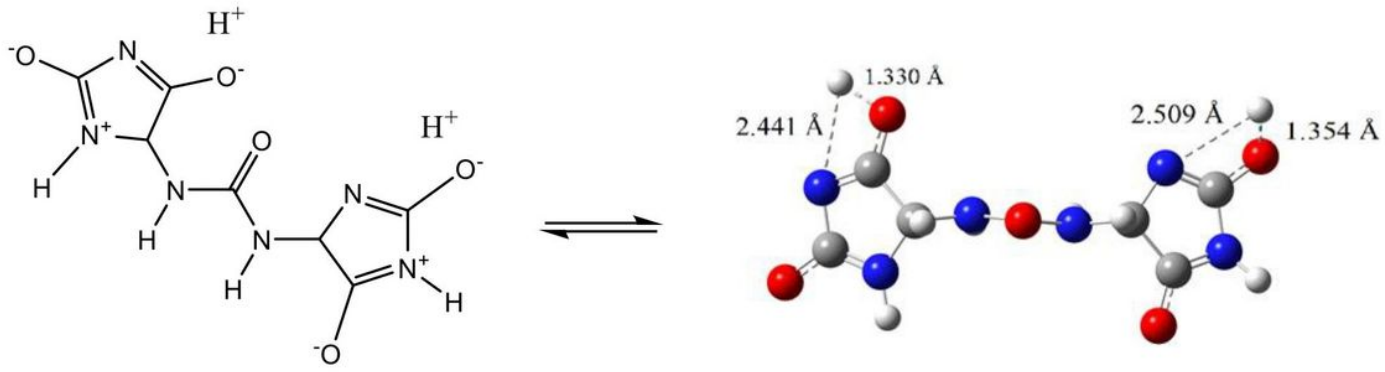

Figure 8

One case of simulated "iminol"/"iminolate" form of 2 with distances between protons and nitrogen or oxygen atoms at B3LYP/6–31G+(d,p); this form seems to induce the electronic transitions (in nm).

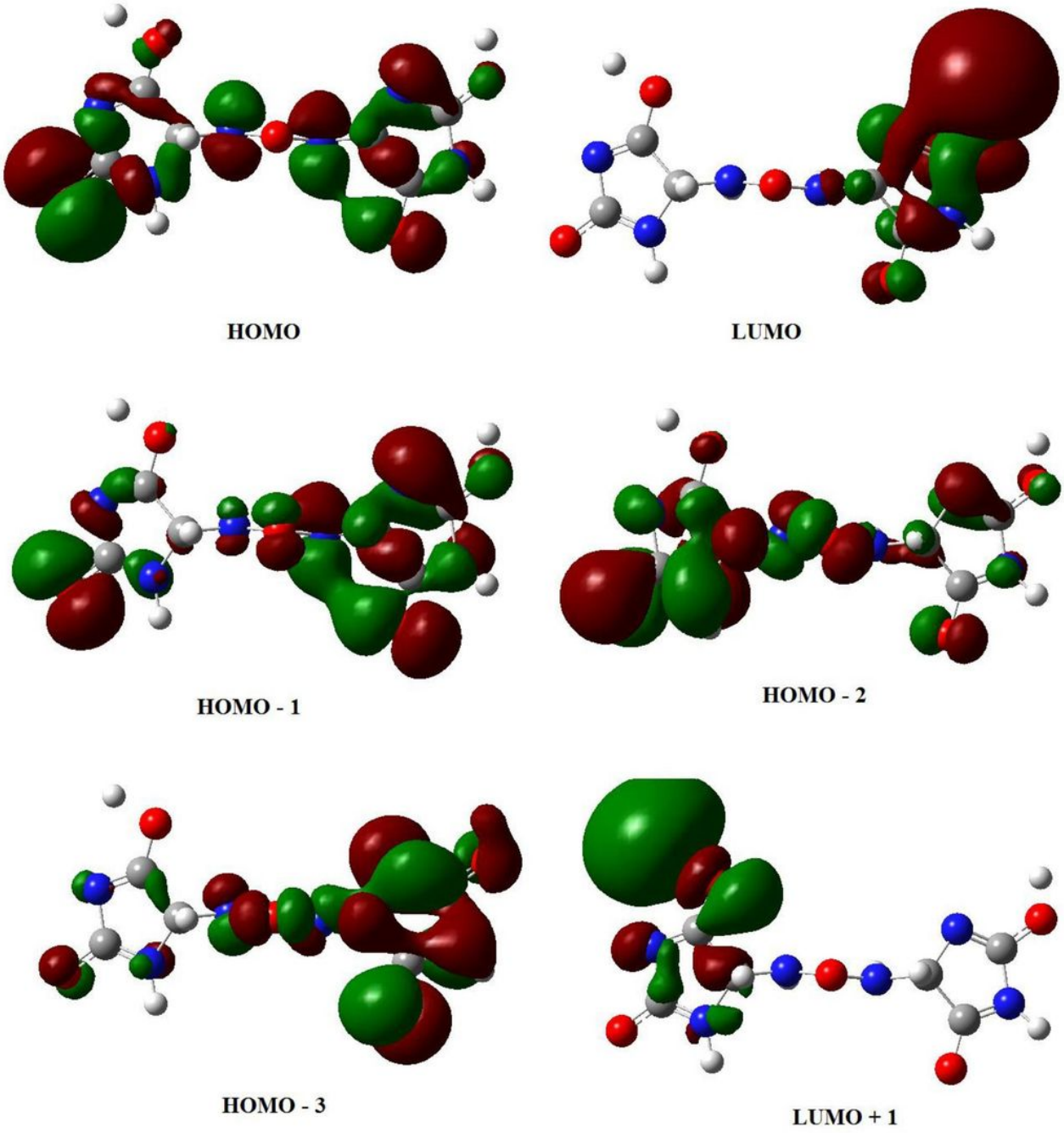

Figure 9

various MOs of 2 involved in electronic transitions, at B3LYP/6–31G+(d,p).

Supplementary Files

This is a list of supplementary files associated with this preprint. Click to download.

- SupportinginformationBMC.pdf